Reviews in Mineralogy & Geochemistry
Vol. 68, pp. 219-246, 2008

Oxygen and Other Volatiles in the Giant Planets and their Satellites

Michael H. Wong
Astronomy Department, University of California
Berkeley, California 94720-3411, U.S.A.
mikewong@astro.berkeley.edu

Jonathan I. Lunine
Lunar and Planetary Laboratory, University of Arizona
1629 E University Blvd., Tucson, Arizona 85721, U.S.A.

Sushil K. Atreya
Department of Atmospheric, Oceanic, and Space Sciences, University of Michigan
Ann Arbor, Michigan 48105-2143, U.S.A.

Torrence Johnson
Jet Propulsion Laboratory, California Institute of Technology
4800 Oak Grove Dr., Pasadena, California 91109, U.S.A.

Paul R. Mahaffy
NASA Goddard Space Flight Center
Greenbelt, Maryland 20771, U.S.A.

Tobias C. Owen
Institute for Astronomy, University of Hawaii
2680 Woodlawn Dr., Honolulu, Hawaii 96822, U.S.A.

Thérèse Encrenaz
LESIA, Observatoire de Paris
Meudon 92195, France

ABSTRACT

Giant planet atmospheric composition and satellite densities provide insights into protoplanetary disk conditions. Abundances of condensable species and noble gases in well-mixed atmospheres can distinguish among several giant planet formation scenarios, and satellite densities are first order measurements of ice:rock ratios. Recent work on protosolar abundances, relying on three-dimensional spectroscopic modeling of the solar photosphere, provides the framework for the interpretation of measurements.

Model densities of protoplanetary disk condensates are shown as a function of carbon partitioning between CO, CH_4 and organics. Comparison with observed satellite densities shows that Saturn's icy satellites are inconsistent with solar composition, and must either have formed in a water-rich environment or have suffered a complex collisional history. The larger satellites of the giant planets are consistent with solar composition, with densities that speak of variation in the partitioning of carbon.

1529-6466/08/0068-0010$05.00 DOI: 10.2138/rmg.2008.68.10

Thermochemical equilibrium calculations predict water as the deepest tropospheric cloud on Jupiter, the planet with the best-constrained bulk water abundance. Yet cloud base pressure levels, remote spectroscopic water vapor measurements, and in situ mass-spectral measurements have all been unable to distinguish conclusively between subsolar and supersolar Jovian bulk water abundances, due to modeling assumptions and/or the spatially-variable water vapor distribution in Jupiter's troposphere. Modeling of images of lightning flashes is consistent with supersolar water abundances.

Galileo probe measurements are consistent with an enrichment factor of 4±2 over the protosolar values for most volatiles other than water (C, N, S, and the noble gases Ar, Kr, and Xe). With that of oxygen unknown, Jupiter's enrichments of other volatiles could be explained in terms of enrichment by heretofore unidentified solar composition icy planetesimals, by planetesimals containing volatiles trapped in water ice clathrates, or by enriched gas in the evolved disk. All models involving delivery of elements by planetesimals require planetesimal formation at temperatures below 40 K, to trap argon and molecular nitrogen. Although atmospheric C/H ratios have been measured for all four giant planets, a conclusive test of the competing formation scenarios cannot be made until O/H is measured on all four planets (extremely difficult on Uranus and Neptune), and abundances of the other volatiles and noble gases are measured for the outer three.

INTRODUCTION

Oxygen-based insights from the outer planets and their moons

As the dominant solid-forming element in a gas of solar composition, oxygen is a primary tracer of early protoplanetary disk conditions. Condensation of gaseous H_2O at low temperature trapped other volatiles along with it, and the overall density of condensates—including water, silicates, and solid carbon—was affected by the partitioning of carbon between CH_4, CO, and carbonaceous forms. Any spatial variability of protoplanetary disk conditions therefore would also have been imprinted on the condensates. This chapter reviews the extent to which early solar conditions can be reconstructed from observations of the oxygen abundances and related volatiles in the giant planets and their moons.

Unfortunately, it is highly likely that the bulk abundance of water in the atmosphere of a giant planet has not yet been measured. Jupiter's water abundance is the best constrained of the outer planets, and a large part of this chapter is a review of attempts to determine the bulk water abundance in this planet. Water in the outer planets was delivered by accretion of solid planetesimals, and these planetesimals indeed fit the profile of "dirty snowballs:" contaminants in the accreted ice resulted in the presence of other volatile gases in the present-day atmospheres of these planets. Temperature and pressure affect both the phase of ice condensed from the disk, as well as the relative abundances of the volatile gases incorporated into this ice, so trace gas abundances illuminate when, where, what, and how the planetesimals formed before their accretion into the giant planets, even if the present-day planetary water abundances are not known. In much the same way, a diner confronted by a bowl containing just tofu cubes and seaweed might infer that it had previously contained miso soup, even if the broth itself had already been consumed.

The densities of outer planet satellites can be interpreted to first order as measurements of their ice-to-rock ratios. A given definition of "protosolar composition gas" permits a certain range of condensate densities consistent with protosolar composition, as a function of the dominant carbon reservoir. Past discussions of solid material formed in the outer Solar System have focused on differences expected between material formed near giant planets, where carbon is generally expected to be in the reduced form (CH_4, with oxygen as H_2O), and material formed in the outer protoplanetary disk, where CO is believed to be the dominant form, with less oxygen available in the form of water due to the solar C/O ratio of about 0.5 (Prinn 1993). The

bulk densities of outer planet satellites thus allow condensate source regions to be inferred, but it seems likely that the carbon budget of the protoplanetary disk also included a high proportion of solid carbon in the form of amorphous carbon grains, macromolecular carbon, and ices of compounds such as methanol, formaldehyde, and carbon dioxide. Solid carbon complicates the interpretation of satellite densities, both because it directly affects condensate density and because it reduces the amount of CO available to sequester oxygen in the gas phase.

In addition to abundance ratios, we also refer to mixing ratios and mole fractions in this chapter. In terms of a number density, n_X, of species X, an abundance ratio such as X/H is simply defined as n_X/n_H; an outer planet atmospheric mixing ratio is defined as n_X/n_{H_2} because H_2 is the major atmospheric component in the observable parts of these atmospheres; and a mole fraction is defined as n_X/n_T, where n_T is the total atmospheric number density.

The protosolar abundances

Our ability to interpret giant planet volatile gas inventories and satellite bulk densities is limited by our knowledge of the protosolar composition. In the case of outer planet moons, the protosolar C/O ratio is critical, since the partitioning of carbon between CH_4 and CO controls the amount of water and thus the density of condensed solids. For the outer planets themselves, the oxygen abundance is not directly measured. Measurements of the abundances of volatile elements originally included with water ice, such as C, N and some noble gases, can be interpreted only with the aid of accurate estimates of the protosolar abundance ratios of these elements.

Most early discussions of the composition of the protoplanetary disk were based on the abundances compiled by Cameron (1981). With Cameron's C and O abundance values, the expected uncompressed density of condensates ranges from 1300 to 1900 kg m^{-3}, depending on the partitioning of carbon between CO and CH_4. This agreed reasonably well with the range of outer planet satellite densities known at the time, particularly for Ganymede and Callisto (Schubert et al. 1986). At the same time, measurements of the methane abundances in the atmospheres of the outer planets were being reported, but oxygen and other volatile gases were still unconstrained. The increasing abundance of methane in these planets with increasing distance from the Sun has been known for several decades (Slipher 1933; Owen 1967; Encrenaz et al. 1974; Lutz et al. 1976). A major revision to the solar values was proposed by Anders and Grevesse (1989), and a review of carbon chemistry by Simonelli et al. (1989) adopted similar values. The decrease in the C/O ratio relative to the previous standard resulted in a smaller range of condensate densities (1400 to 1600 kg m^{-3}). The Anders and Grevesse (1989) standard was used to interpret the deep nitrogen and sulfur abundances discovered by the Galileo probe upon its descent into Jupiter's atmosphere (e.g., Folkner et al. 1998; Niemann et al. 1998).

Recent advances in 3-dimensional spectroscopic modeling of the solar photosphere have resulted in updated abundances of C, O, N, and other elements (Grevesse et al. 2005; Asplund et al. 2004; Allende Prieto et al. 2002). The revised oxygen abundance is about 50% lower than the previously accepted Anders and Grevesse (1989) value and, along with a change in carbon abundance, results in both greater overall condensate densities as well as a greater range (1500 to 2200 kg m^{-3}) as a function of CO/CH_4 ratio. Protosolar abundances are slightly greater than these photospheric values, due to the effects of gravitational settling (Turcotte et al. 1998; Turcotte and Wimmer-Schweingruber 2002; Lodders 2003). Throughout this review, we interpret enrichments using both Anders and Grevesse (1989) and Grevesse et al. (2005) solar compositions, to illustrate the very large effect of uncertainties in the solar abundance determinations.

The new abundances, although based on improved solar photospheric modeling, raise issues between solar structure modeling and helioseismic results. A recent assessment of this "solar model problem" was made by Drake and Testa (2005) in light of new measurements of the Ne/O ratio in the coronae of active solar-like stars with the Chandra X-ray Observatory.

They conclude that, if the higher neon/oxygen ratio of 0.4 in these stars is adopted for the Sun, the solar models can match helioseismic sound speeds using the new O and C abundances. However, Grevesse et al. (2005) prefer a solar Ne/O ratio of 0.15, based on spectroscopic observations of the Sun's corona and on direct sampling of solar wind material. They note that the lower Ne/O value is in better agreement with the Ne/O in the local galactic medium and with theories of type II supernova nucleosynthesis. In any case, the sound speed discrepancies between helioseismic and solar model results, which are at the 3% level, are mostly confined to the interface between the radiative and convective zones of the Sun, a region that is difficult to accurately characterize with a one-dimensional model like the standard solar model (Christensen-Dalsgaard 2006). Thus, we adopt the Grevesse et al. (2005) protosolar O/H and C/H values of 5.13×10^{-4} and 2.75×10^{-4}, respectively, in this work.

MEASURING OXYGEN IN JUPITER'S ATMOSPHERE

Oxygen in the observable part of Jupiter's atmosphere is present almost exclusively in the form of H_2O. Two sources of atmospheric water have been identified: an internal reservoir; and an external source, first identified by the Infrared Space Observatory (ISO) satellite (Feuchtgruber et al. 1997; Coustenis et al. 1998). An external source of water has also been found in the stratospheres of the other giant planets and Titan. The external source of oxygen might have two origins: a local contribution from satellites and/or rings; or an interplanetary origin, from comets, including comet Shoemaker-Levy 9 in the case of Jupiter (Lellouch et al. 2002), and/or micrometeoritic infall. In order to constrain formation models of the giant planets, we need to determine the oxygen content of the internal reservoir. Attempts to measure the bulk abundance of water in Jupiter have been unsuccessful to date. Water condenses deep below Jupiter's upper cloud decks, and although breaks in the cloud layers allow glimpses of deeper levels, local meteorology also reduces the water column abundance in these areas, so that the deep well-mixed water mixing ratio is inaccessible to both remote sensing and to the Galileo Probe. In this section, we review Jupiter's cloud structure, in order to understand its effect on measurements of water. We look at the results of the Galileo Probe Mass Spectrometer (GPMS), which provided the only *in situ* measurement of water on Jupiter, and then review methods of inferring water abundances using remotely sensed data sets.

Structure of the cloud layers

Unlike the Earth's troposphere, in which only water clouds condense, Jupiter's troposphere hosts clouds of at least three different compositions (e.g., Weidenschilling and Lewis 1973). The top two layers, which are most accessible to remote sensing, are composed of ammonia ice and ammonium hydrosulfide (or some other combination of ammonia and hydrogen sulfide). The water cloud is seldom glimpsed, since it lies deeper than these higher clouds. The exact pressure level at which water condenses depends on the pressure-temperature structure of the atmosphere, as well as the abundance of water vapor in the atmosphere.

Figure 1 shows the maximum depth of the water cloud base (otherwise known as the lifting condensation level) as a function of water enrichment relative to solar. We first calculated the saturation vapor pressure of water for the temperature-pressure structure measured by the Galileo Probe Atmospheric Structure Instrument (Seiff et al. 1998). The saturation vapor pressures are expressed in Figure 1 in terms of solar enrichment, where the black curve corresponds to solar O/H from Anders and Grevesse (1989), and the grey curve corresponds to the Grevesse et al. (2005) protosolar O/H. Thus, for solar O/H, the deepest possible cloud would form at about 5 bar. Cloud bases at lower pressures (higher altitudes) would also be expected, since condensation and circulation can act to deplete water locally. But in an atmosphere with solar O/H, clouds could not form deeper than about 5 bar, because localized water enrichments over the well-mixed value would be difficult to create and maintain.

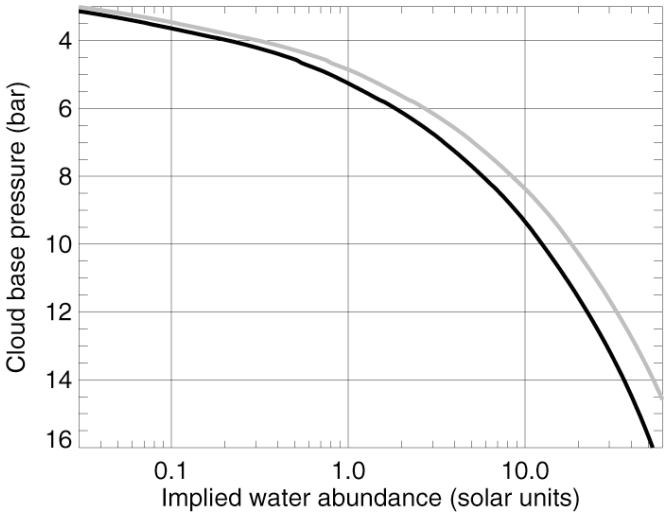

Figure 1. Cloud base pressure (or lifting condensation level) as a function of bulk water abundance. Black curve is for solar O/H from Anders and Grevesse (1989), grey curve is for protosolar O/H from Grevesse et al. (2005). We used the observed temperature-pressure profile from the Galileo Probe Atmospheric Structure Instrument (Seiff et al. 1998), and determined the saturated water vapor pressure over an aqueous ammonia solution at each level (Atreya and Romani 1985) based on laboratory data for the 273-363 K range (Wilson 1925; Linke 1965).

Galileo Probe Mass Spectrometer water mixing ratio measurements

One of the primary goals of the Galileo Probe Mass Spectrometer (GPMS) experiment was to descend below the expected water cloud base near 5 bar and measure the deep, well-mixed water mixing ratio (Niemann et al. 1996). However, the probe entry site was in the vicinity of a 5-μm hotspot, a region of atypical meteorology characterized by reduced mixing ratios of condensable volatiles. The deepest water mixing ratio measured by the GPMS was $(4.9 \pm 1.6) \times 10^{-4}$ in the 17.6-20.9 bar pressure region (Wong et al. 2004). Evidence from numerous sources (see below) strongly suggests that the bulk water abundance remains unmeasured due to the probe's entry into a 5-μm hot spot.

These 5-μm hot spots are regions of "unusual clarity and dryness" (Orton et al. 1998). Early photometry of Jupiter in the 5-μm wavelength region found that the north equatorial belt was much brighter than the rest of the planet, with fluxes too high to be reflected sunlight (Westphal 1969). Higher resolution studies revealed that even within the restricted latitude range of the north equatorial belt (approximately 8-18° N planetographic latitude in Smith et al. 1979), localized hot spots were responsible for much of the radiation (e.g., Keay et al. 1973; Armstrong et al. 1976). The radiation is due to thermal emission from as deep as 5 bar in Jupiter's atmosphere, within a spectral window of low gas opacity bracketed by NH_3 absorption longward of 5.2 μm and CH_4 absorption shortward of 4.5 μm (Atreya 1986). Clarity therefore modulates Jupiter's 5-μm brightness, and a strong correlation with dryness was demonstrated by the longitude-resolved variation of the ammonia mixing ratio presented in Sault et al. (2004).

Figure 2 summarizes the water vapor mixing ratio measurements of the GPMS. Each data point is derived from a single measurement of counts at the atomic mass-to-charge ratio of 18, characteristic of singly-ionized H_2O. To convert these counts to an atmospheric mixing ratio, we divided the counts at mass 18 by the counts measured for a gas with constant mixing ratio, such as helium or methane. Other considerations that affect the data are the contribution to

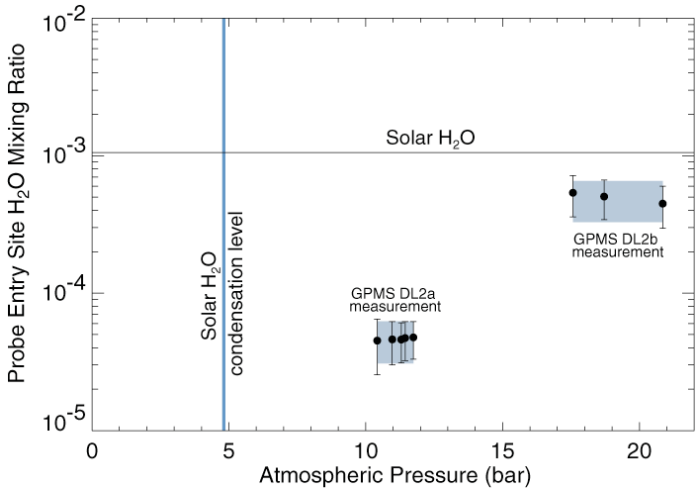

Figure 2. Galileo Probe Mass Spectrometer (GPMS) water measurements, from Wong et al. (2004). Individual data points have been averaged to give mixing ratios of $(4.7 \pm 1.5) \times 10^{-5}$ over the 11-11.7 bar pressure range and $(4.9 \pm 1.6) \times 10^{-4}$ over the 17.6-20.9 bar range. The horizontal line shows the protosolar water abundance using the Grevesse et al. (2005) O/H ratio, and the vertical line shows the lifting condensation level for a solar water abundance. The order of magnitude increase from 11 to 20 bar, much deeper than the lifting condensation level, indicates the strong effect of local meteorology on the measured water mixing ratio.

mass 18 from doubly ionized argon; pressure variation of the calibration constant relating count ratios and mixing ratios; signal nonlinearity; and instrumental background signals.

Although the corrections for these effects are described more completely in Niemann et al. (1998) and Wong et al. (2004), the instrumental background signal is of particular note for this discussion. Shaded boxes in Figure 2 show water measurements for two pressure ranges: 11-11.7 bar (called DL2a) and 17.6-20.9 bar (called DL2b). These pressure ranges correspond to times during the GPMS experiment when the mass spectrometer was directly sampling Jupiter's atmosphere through one of two independent gas pressure reduction systems. Between the DL2a and DL2b experiments, the mass spectrometer was exposed to a special cell in which gases were enriched with respect to hydrogen, mainly for the purpose of measuring isotopic ratios. During this enrichment cell experiment, count rates for enriched gases (including H_2O) shot up, and a decaying residual background signal was observed in the DL2b experiment just afterwards. Because of this large background signal, Niemann et al. (1998) reported only an upper limit for the 17.6-20.9 bar H_2O mixing ratio, but the current value is based on detailed calibration experiments done at NASA Goddard Space Flight Center, using the flight spare version of the GPMS, in order to simulate descent conditions and model the decaying background component (Wong et al. 2004).

The error bars in Figure 2 show the estimated uncertainties in each mixing ratio data point due to all sources of error, including this background signal. The decrease in the central values of the 17.6-20.9 bar points with increasing pressure implies that there is still a residual background signal (memory from the enrichment cell operation) that has not been entirely removed. However, within the estimated uncertainties of the three data points between 17.6-20.9 bar, we cannot distinguish between a factor of two increase over this pressure range, a factor of two decrease, or a constant value over the whole pressure range. Increases or decreases of greater than a factor of two over this range do not fall within the estimated uncertainty. The data at 17.6-20.9 bar are statistically consistent with a linear increase in water that extrapolates

to 1.7 × solar abundance[1] at 20 to 40 bar, depending on calibration constant uncertainties (Wong and Mahaffy 2001). Due to the magnitude of the estimated uncertainties, we interpret the GPMS H_2O measurements as two single data points: one at about 11 bar, and one at about 19 bar, demonstrating an order of magnitude increase over the 11-20 bar range. It is likely that the water mixing ratio continues to increase even further with depth, well beyond the level from which the last signals were received from the probe at 22 bar, given the unusual meteorology of the probe entry site.

The probe entry site: A 5-μm hot spot

A look at the pressure-dependent variation of condensable volatile mixing ratios in the probe entry site strongly suggests that the deep GPMS measurement does not represent Jupiter's bulk oxygen abundance. Mixing ratios of all three condensable volatiles were observed to increase with depth, with the ammonia and H_2S mixing ratios eventually leveling off at their deep well-mixed values. For ammonia, this constant mixing ratio was achieved at about 8 bars (Folkner et al. 1998). This 8-bar equilibration level is at a much greater pressure than the lifting condensation level of about 1 bar for the ~5-6 × solar bulk nitrogen enrichment relative to Grevesse et al. (2005) values measured by the probe's radio signal attenuation (Folkner et al. 1998) and by the GPMS (Niemann et al. 1998; Mahaffy et al. 1999; Atreya et al. 2003; Wong et al. 2004). The GPMS also measured the increase of the H_2S mixing ratio with depth. This gas reached its equilibration level somewhere within the 12-16 bar region (Niemann et al. 1998; Atreya et al. 1999, 2003; Wong et al. 2004), where the GPMS was not sensitive to the ambient atmosphere due to the enrichment cell experiment. The main loss process for H_2S is condensation into the NH_4SH cloud, which should occur at about 2.6 bar for an approximately 3 × solar H_2S enrichment (Atreya et al. 1999). Thus, the staggered equilibration levels for ammonia and for H_2S occur in the same order as the staggered condensation levels for the clouds formed by these gases. Water should then reach its equilibration level at the highest pressure of all, since its lifting condensation level is deepest.

No quantitatively precise explanation exists for the probe entry site condensable volatile profiles, with their equilibration levels occurring much deeper than their expected condensation levels. There is, however, an obvious pattern: based on lifting condensation levels, the ammonia clouds should form at about half the pressure of the NH_4SH clouds, and the pressure of the observed ammonia mixing ratio equilibration level was also about half the pressure of the H_2S mixing ratio equilibration level. Given this pattern, and the fact that the water lifting condensation level is in the 5-6 bar range for water in the 1-3 × solar range (Fig. 1), it is reasonable to expect that the water mixing ratio would not reach a constant value until pressures much deeper than the H_2S equilibration level, somewhere in the 12-16 bar region. A simple scaling based on the fact that the pressure at the water condensation level is about three times higher than the pressure at the NH_4SH condensation level would lead to the expectation that the water equilibration level in the probe entry spot is as deep as 30-45 bar, roughly the same level at which the GPMS data would extrapolate to a solar water mixing ratio (Wong and Mahaffy 2001). There is, however, no physical basis on which to expect the same scaling law to apply to the lifting condensation levels and the probe entry site mixing ratio equilibration levels for all three condensable volatiles. In fact, a comparison of condensable volatile mixing ratios at the ammonia and H_2S equilibration levels in the probe entry site shows that these mixing ratios do not scale this simply (Wong et al. 2004).

Two models of 5-μm hotspots provide qualitative agreement with the condensable volatile mixing ratio profiles at the probe entry site. The 3-dimensional, nonlinear model of Showman and Dowling (2000) simulated long-lived structures with drift rates and longitudinal spacings

[1] Using Grevesse et al. (2005) solar abundances, or 1 × solar abundance using Anders and Grevesse (1989).

that matched 5-μm hot spot observations, and it successfully reproduced the cloud-top velocity field measured for a Jovian 5-μm hot spot. But, due to computational limitations, this code could only model vertical shifts of condensable volatile profiles to about 10 bar. The Rossby wave hypothesis of Friedson (2005) agrees with the spacing between the 5-μm hotspots and the intervening spectroscopically identifiable ammonia ice clouds of Baines et al. (2002), finding pressure variations along isentropes of up to a factor of 40 within the propagating wave. Although neither of these models accurately matches all the observed characteristics of 5-μm hot spots, they are sufficiently realistic to provide convincing evidence that the water mixing ratio sampled by the Galileo probe is not characteristic of the well-mixed water abundance in Jupiter's atmosphere.

Spectroscopic measurements of Jovian water

Remote sensing measurements tell us about the water abundance in Jupiter through two main methods: direct spectroscopic analysis of water lines; and measurements of cloud depths. Unfortunately, neither method has revealed the bulk oxygen abundance of Jupiter. We briefly review remote sensing results here, since these results set valuable lower limits on the water abundance and may also inform future attempts to measure water mixing ratios in Jupiter.

Modeling of water lines in the 4.5-5 μm region of Jupiter's thermal infrared spectrum allows the retrieval of water vapor mixing ratios in the troposphere. Spectral data from the Voyager Infrared Radiometer Interferometer and Spectrometer (Voyager IRIS; Bjoraker et al. 1986a; Drossart and Encrenaz 1982; Kunde et al. 1982; Lellouch et al. 1989a,b), the Kuiper Airborne Observatory (KAO; Bjoraker et al. 1986a,b), ISO's Short Wavelength Spectrometer (ISO/SWS; Roos-Serote et al. 1999), and Galileo Near Infrared Mapping Spectrometer (Galileo NIMS; Roos-Serote et al. 1998, 1999, 2000, 2004; Irwin et al. 1998, 2001; Nixon et al. 2001) have been interpreted to yield estimates that vary significantly with data set and with modeling approach, but there is a broad consensus that subsaturated water vapor mixing ratios are widespread. No evidence is found for water vapor mixing ratios in excess of the solar abundance at pressures from which the 5-μm emission emanates. Within Jupiter's 5-μm window, the deepest level of penetration (where τ=1) is limited to about 6 bar by pressure-induced hydrogen absorption (e.g., Bjoraker et al. 1986b).

But these measurements are not signs of a low bulk oxygen abundance, because they are influenced by correlated meteorological patterns and spectral opacity in Jupiter's atmosphere. The overall brightness of Jupiter's 5-μm spectral window is strongly modulated by cloud opacity near 1.5 to 2 bar (e.g., Bjoraker et al. 1986b; Roos-Serote et al. 1998; Irwin et al. 1998; Nixon et al. 2001), so spatially-averaged spectra will be weighted more towards regions with low 2-bar cloud opacity. Longitudinally resolved thermal microwave images of Jupiter demonstrate that this low cloud opacity is correlated with local depletions of ammonia (Sault et al. 2004; Wong et al. 2006a), and GPMS data show that all condensable volatile gas abundances (not just ammonia) were found to be depleted to very deep levels in at least one 5-μm hotspot. Roos-Serote et al. (2000) used a multispectral NIMS image of a 5-μm hotspot to determine that water relative humidity was very low (< 1%) across most of the region, but isolated regions nearby had very high water relative humidity, approaching saturation. These humid regions had much lower 5-μm radiances, by at least an order of magnitude, and also showed evidence of vigorous convective activity in the Galileo imaging data. Thus, it is clear that the lower spatial resolution Voyager IRIS and KAO observations are biased toward relatively cloud-free regions with low water relative humidity, and we cannot determine the amount of water vapor in the more humid regions without independently knowing the filling factor between humid and dry regions. Lunine and Hunten (1987) found that this filling factor must be 2% or less to match the 5-μm observations.

Jupiter's spectrum in the 5-μm window is also affected by the presence of a water cloud. Carlson et al. (1993) modeled IRIS 5-μm spectra in the North Equatorial Belt with a detailed

radiative transfer code including multiply-scattering, thermally-emitting clouds with spectrally-dependent extinction, and cloud base levels determined by the assumed condensable volatile abundances. They could only fit the observed spectra (which included 5-μm hot spot spectra) by including a water cloud at the pressure level corresponding to a 2 × solar water enrichment. Roos-Serote et al. (1999) compared the IRIS spectra used in Carlson et al. (1993) with spectra from Galileo NIMS and ISO/SWS. They found an anomalous slope in the IRIS spectra, which could have tricked the Carlson et al. (1993) model into requiring a water cloud. Further study of water cloud effects on the NIMS 5-μm spectral characteristics (Roos-Serote et al. 2004) revealed that this spectral region could be fit with either (a) no clouds between 2.5 and 8 bars, in which case the water vapor relative humidity never exceeds 10%, resulting in subsolar O/H; or (b) clouds, as predicted by thermochemical models for a given composition, but with no significant opacity between 2.5 and 5 bars allowed. This finding is weakly suggestive of supersolar water abundances, since only such abundances could result in cloud condensation at pressures deeper than 5 bar.

Imaging results are not compatible with a complete absence of clouds deeper than 3 bar. In Galileo imaging data, deep clouds were seen adjacent to the much higher tops of optically thick plumes associated with strong convection (Banfield et al. 1998; Gierasch et al. 2000). With cloud-top pressures in excess of 4 bar, these deep, thick clouds can only be composed of water. But since only the tops of these optically thick clouds could be seen at pressures of 4 bar or more, these clouds cannot directly imply water mixing ratios greater than those measured by the GPMS. Fifteen clouds were tracked as they moved through clearings associated with 5-μm hotspots in Cassini imaging data (Li et al. 2004). It seems very likely that these clouds were truly water clouds, because their measured speeds indicate that these clouds are at different altitudes from the opening in the 2-bar cloud layer that defines the 5-μm hotspots, and because the filter set used in the study ruled out the possibility that these clouds were instead located above the cloud deck framing the 5-μm hotspots. Although this study was unable to determine the pressure level of the deep clouds, it describes clouds at $P > 4$ bar. In combination with the previous result that cloud opacity is not significant between 2.5 and 5 bar (Roos-Serote et al. 2004), these clouds therefore should be located at 5 bar or deeper, again suggesting solar or supersolar water abundances.

Spectroscopic measurements of CO may also be used to infer the bulk oxygen abundance in Jupiter indirectly. As mentioned before, in the observable troposphere, water is the thermochemical equilibrium species of oxygen. But at temperatures exceeding 1000 K, the CO/H_2O ratio increases beyond the part per billion level. Observations of CO at the part per billion level in the troposphere (e.g., Bjoraker et al. 1986b; Noll et al. 1988, 1997; Bézard et al. 2002) therefore indicate that CO is being brought up from Jupiter's deeper interior faster than it can reach chemical equilibrium with H_2O. The observed mixing ratio of CO is then a function of the time constant for mixing, the reaction rates and pathways for chemical exchange between CO and H_2O, and the total abundance of oxygen. Fegley and Lodders (1994) found that the observed tropospheric CO content was in good agreement with an O/H ratio of 2×10^{-3}, which is 2.3 × solar using Anders and Grevesse (1989) values, or 3.4 × solar using Grevesse et al. (2005) values. Bézard et al. (2002) also modeled diffusion of CO from the deep interior, but used different reaction pathways and a different treatment of eddy mixing. They find 0.2-9 × solar O/H using Anders and Grevesse (1989), or 0.3-13 × solar O/H using Grevesse et al. (2005).

Lightning on Jupiter

Imaging studies of Jovian lightning provide possibly the best evidence that Jupiter's oxygen abundance is at least solar. Since reflected sunlight drowns out lightning flashes on Jupiter's dayside, the lightning data set consists of images from spacecraft positioned to observe the planet's nightside: the Voyagers (e.g., Cook et al. 1979;Smith et al. 1979; Borucki et al. 1982), Galileo (Little et al. 1999; Dyudina et al. 2002), and Cassini (Dyudina et al. 2004). Lightning

on Jupiter is almost certainly generated in water clouds. Levin et al. (1983) argued that the ammonia cloud probably cannot generate sufficient charge separation, partly due to the low mass loading of the cloud. Charge separation is also inhibited by the reduced conductivity of ammonia ice, mainly due to the much lower temperature at the ammonia cloud level compared to temperatures in the deeper and warmer NH_4SH and water cloud levels. Thermodynamic models predict that the NH_4SH cloud layer should have a similar mass loading to the ammonia cloud, but the water cloud should be about an order of magnitude more massive (e.g., Atreya et al. 1999). Levin et al. (1983) conclude that the mass loading, simultaneous existence of liquid and solid phases, and vigorous convection combine to make the water clouds the ideal candidates for lightning generation.

Lightning strikes in the water cloud are blurred in spacecraft images due to scattering by intervening cloud particles. Models relating the size (width at photometric half-maximum) of the lightning spots to the depth of the lightning strokes beneath the cloud tops in Voyager and Galileo images agree that the lightning must be located at pressures of 5 bar or more (Borucki and Williams 1986; Little et al. 1999; Dyudina et al. 2002). Since Jovian lightning strokes must be intracloud, or possibly extending upwards from the cloud (Levin et al. 1983), clouds must be present at the depths found for the lightning strokes. According to Figure 1, lightning at 5 bar or deeper therefore implies a water abundance greater than or equal to solar. The deepest flashes found by Dyudina et al. (2002) occur at 10 bar or deeper, which would imply an oxygen enrichment of at least 9 times solar. Although the degree of the enrichment depends on the accuracy of the photometric model, the agreement between multiple models that the lightning is at 5 bar or deeper is, nevertheless, a compelling result.

Voyager and Galileo lightning images were taken with wideband filters, but the Cassini lightning observations were taken in a narrow filter optimized to detect H_α emission. Simulated Jovian lightning spectra (Borucki et al. 1996) show strong emission at this wavelength, with broader line emission produced at a pressure of 5 bar than at 1 bar. Dyudina et al. (2004) used the lightning frequency and brightness distributions determined from Voyager and Galileo observations, along with the expected increase in lightning signal-to-noise ratio due to the narrow H_α filter on Cassini, to predict the number of lightning strikes expected to be found in Cassini imaging data. They found 10-100 times less lightning in Cassini images than expected. Their favored explanation for this discrepancy was that lightning production at depths greater than the 5 bar used in the Borucki et al. (1996) study resulted in greater spectral broadening of the H_α emission, rendering most of the lightning strikes undetectable by the Cassini imager. Although it is possible that lightning stroke frequency was reduced by one or two orders of magnitude during the Cassini encounter compared to the Voyager and Galileo observations, it seems more likely that the unexpectedly low H_α emission is an indication of lightning production at pressures deeper than 5 bar, which in turn implies a supersolar water abundance.

Oxygen isotopes in Jupiter

Oxygen isotopic ratios for Jupiter are completely unknown. The GPMS was unable to resolve oxygen isotopic signatures due to mass interference from other gases. The $H_2{}^{17}O$ mixing ratio could not be determined from the signal at the mass-to-charge ratio of 19, due to interference from $^{38}Ar^{++}$ as well as a relatively high level of background signal (Fig. A.3 in Wong 2001). Although solar oxygen isotopic ratios would suggest a stronger and more easily measured signal from $H_2{}^{18}O$, any signal from this molecule, at mass 20, would have been overpowered by neon.

Summary of Jovian oxygen

The most important conclusion from this review of all the available data is that the oxygen abundance on Jupiter remains unknown. We have an excellent lower limit from the Galileo Probe mass spectrometer, but it is only a limit. Table 1 summarizes the oxygen abundance

estimates determined from the numerous investigations detailed above. All of the inferred oxygen abundances are, unfortunately, heavily model-dependent, heavily influenced by meteorology and spatial inhomogeneity, or both. The best way to overcome these obstacles would be to return to Jupiter with multiple probes entering the atmosphere at different locations, and operating to depths of 50-100 bar (Atreya and Wong 2005). Being technologically challenging and expensive, such a mission is far into the future. In the meantime, help is on the way in the form of Juno! The Juno Polar Orbiter spacecraft will use passive microwave radiometry to map water on the planet to atmospheric pressure levels exceeding 100 bars. The findings of the Juno mission will be helpful in guiding the more ambitious multiprobe mission to Jupiter, where simultaneous measurements of all other key elements could also be carried out.

OUTER PLANET VOLATILE GASES

Although knowledge of the oxygen abundance on Jupiter is crucial for construction of a reasonable formation scenario for Jupiter and the outer planets, information about other volatile gases on the outer planets can inform the discussion. For all the outer planets, the atmospheric mixing ratio of methane, the primary reservoir of carbon, has been measured. For Jupiter, the Galileo Probe also yielded determinations of Jupiter's abundances of nitrogen, sulfur, and noble gases. In this section, we discuss measurements of volatiles on Jupiter and the outer planets, and finally we relate this information to conditions in the early solar system and to the formation of the giant planets.

Oxygen and other heavy element enrichments in Jupiter

As discussed in the previous section, there is no evidence that the GPMS measured Jupiter's bulk water abundance. Figure 3 summarizes the GPMS measurements of Jupiter's volatile and noble gases. Except for water, the data are consistent with a 3 × solar enrichment within the estimated uncertainties, using the solar composition of Anders and Grevesse (1989). The enrichments are more uneven if Grevesse et al. (2005) values are used, with C/H = 4.3 ± 1.0 × solar, N/H = 4.9 ± 1.9 × solar, S/H = 2.9 ± 0.7 × solar, and the noble gases Kr and Xe are 2-2.5 × solar. The revised protosolar Ar abundance results in a Jovian argon enrichment of 5.4 ± 1.1 × solar. Despite this non-uniformity, it is safe to say that the heavy elements are enriched

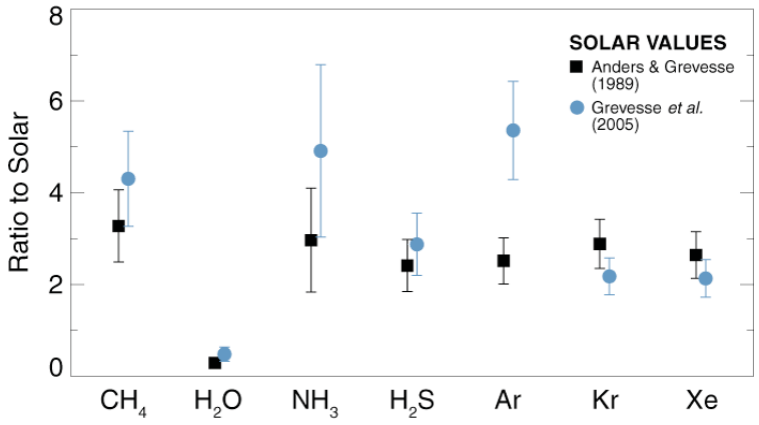

Figure 3. Galileo Probe Mass Spectrometer measurements of volatile and noble gases (from Mahaffy et al. 2000 and Wong et al. 2004). Error bars show uncertainties in the GPMS mixing ratio values, and comparison between Anders and Grevesse (1989) solar abundances (squares) and Grevesse et al. (2005) protosolar abundances (circles) gives an estimate of the effect of uncertainties in solar abundance values.

Table 1. Summary of measurements relating to the determination of Jupiter's water abundance.

Measurement technique	Jovian O/H relative to solar		Strongly affected by model assumptions?[2]	Strongly affected by H_2O spatial distribution?[3]	References
	Anders & Grevesse (1989)[1]	Grevesse et al. (2005)[1]			
GPMS	0.29 ± 0.09	0.48 ± 0.16		×	Niemann et al. (1998), Wong et al. (2004)
5-μm spectroscopy (gas)	0.02	0.03		×	e.g., Bjoraker et al. (1986a,b), Roos-Serote et al. (1999, 2000), also see text
5-μm spectroscopy (clouds)	subsolar, or ≥ 1	subsolar, or ≥ 1.7	×	×	Roos-Serote et al. (2004), also see text
Clouds at $P \geq 4$ bar	> 0.2	> 0.3			Banfield et al. (1998), Gierasch et al. (2000), Li et al. (2004)
Internal CO source	2.3, or 0.2-9	3.8, or 0.3-15	×		Fegley and Lodders (1994), Bézard et al. (2002)
Depth of lightning	> 0.7	> 1.2	×		Little et al. (1999), Borucki and Williams (1986)
Depth of lightning	> 9	> 15	×		Dyudina et al. (2002), Dyudina et al. (2004), see text

[1]Solar O/H = 8.53×10^{-4} in Anders and Grevesse (1989) and protosolar O/H = 5.13×10^{-4} in Grevesse et al. (2005).
[2]See text for details about how these measurements are modeled to infer water abundances.
[3]Observations are biased towards regions with lower water vapor mixing ratios, so the deep well-mixed abundance of water is not measured.

at Jupiter, by a factor of 4 ± 2 × solar, even using the latest values of the protosolar elemental abundances (Owen and Encrenaz 2006).

Although GPMS measurements for many of these abundances are unique, independent confirmation exists for ammonia and methane mixing ratios in Jupiter's atmosphere. Ammonia's mixing ratio is highly spatially variable on Jupiter, so only in the probe entry site has the deep well-mixed ammonia abundance been measured. Folkner et al. (1998) modeled the attenuation of the probe-to-orbiter radio signal as the probe descended, finding that the ammonia mixing ratio increased with depth until about the 8-bar pressure level, where it reached a mole fraction of 700 ± 100 ppm. The enrichment over solar abundance corresponding to this value is 3.6 ± 0.5 (Anders and Grevesse 1989) or 6.0 ± 0.9 (Grevesse et al. 2005). The result from the probe signal attenuation is slightly larger than the GPMS measurement quoted above (see also Fig. 3 and Wong et al. 2004).

Jupiter's methane abundance is much easier to constrain by remote sensing, since the atmosphere is too warm for methane condensation, leaving the tropospheric mixing ratio constant and spatially homogeneous. The GPMS-derived methane mixing ratio of 2.4 ± 0.6 × 10^{-3} (Wong et al. 2004) compares well with numerous methane mixing ratios derived from remote sensing. Gautier et al. (1982) derived a mixing ratio of 1.95 ± 0.22 × 10^{-3} from Voyager IRIS data, and Knacke et al. (1982) used ground-based observations in the 1100-1200 cm^{-1} spectral range to obtain a mixing ratio of 2.5 ± 0.4 × 10^{-3}. Kunde et al. (2004) presented the first detection of CH_4 rotational lines in spectra acquired by Cassini's Composite Infrared Spectrometer (CIRS), confirming previous methane abundance determinations.

Volatile enrichments in the other outer planets

Like Jupiter, Saturn is composed primarily of hydrogen and helium, so its composition can also be usefully discussed in terms of elemental enrichments with respect to hydrogen. Since methane does not condense on this planet, its mixing ratio should be constant within the troposphere. Numerous spectroscopic studies have yielded methane abundances (Buriez and de Bergh 1981; Courtin et al. 1984; Karkoschka and Tomasko 1992; Kerola et al. 1997). The Cassini CIRS investigation improved on these estimates by allowing a derivation of tropospheric CH_4 without *a priori* haze and temperature profile assumptions (Flasar et al. 2005; Orton et al. 2005). The CIRS methane mixing ratio of 5.1 ± 1.0 × 10^{-3} corresponds to a supersolar enrichment of 7.0 ± 1.4 (Anders and Grevesse 1989) or 9.3 ± 1.8 (Grevesse et al. 2005), about a factor of two larger than for Jupiter. Modeling of Saturn's thermal microwave spectrum (de Pater and Dickel 1991) yields more modest enrichments of ammonia of 2.2 × solar (Anders and Grevesse 1989) or 3.1 × solar (Grevesse et al. 2005), for pressures of 3 bar or more. However, 3 bar in Saturn's atmosphere is expected to be within the condensation region for NH_4SH, where ammonia mixing ratios may be variable. Thus, the microwave-derived NH_3 mixing ratio should be regarded as a lower limit for Saturn's bulk nitrogen component. Tropospheric water has been detected at 5 μm in Saturn with ISO (de Graauw et al. 1997), but, as in the case of Jupiter, the very low measured abundance ($H_2O/H_2 = 2 \times 10^{-7}$) suggests a strong undersaturation effect, probably associated with dynamical effects within dry regions of subsidence. Convection in Saturn's atmosphere is not well understood, however, primarily because Saturn's cooler atmosphere (compared with Jupiter) means that its clouds condense at higher pressures. Obscured by overlying haze, the clouds are more difficult to observe and therefore less useful as tracers of dynamics. Hydrogen sulfide and the noble gases have not been measured for Saturn, so the methane mixing ratio and the upper limit for ammonia provide the best constraints on the volatile enrichments in Saturn's atmosphere. The only other heavy elements detected at Saturn—P, As, Ge and Si—are all disequilibrium species, and thus are not good indicators of the heavy element enrichment factor.

Unlike Jupiter and Saturn, Uranus and Neptune have compositions that are not dominated by hydrogen and helium. Based on observed gravitational moments and other basic parameters,

Podolak et al. (2000) conducted a Monte Carlo search of acceptable density profiles for these planets. In terms of the basic Solar System building blocks of rock, ice, and gas (or refractory, volatile, and gas components), estimates of the proportions of gas present in Uranus and Neptune depend on assumptions about the planets' overall compositions. Thus, Podolak et al. (2000) found an absolute maximum proportion of gas (by mass) of about 30% for Uranus and Neptune, under the unrealistic assumption that the planets were composed entirely of rock and gas. Models constructed assuming a rocky core surrounded by a mantle composed of ice and gas, and constrained by available equation of state data, are reviewed by Hubbard et al. (1995) and Guillot (2006). These models generally agree that the proportion of gas (by mass) in these planets is around 5-15%, so the O/H ratio in these planets should be very large.

The only heavy element abundance measured at Uranus and Neptune is that of carbon, whose value relative to hydrogen ranges from 18-50 × solar at Uranus and 28-63 × solar at Neptune, derived from Voyager radio occultations (Lindal et al. 1987; Lindal 1992) and from ground-based optical spectroscopy (Baines et al. 1995). On both planets, methane condenses at approximately the 1-bar level (Atreya and Wong 2005), which is consistent with the Voyager observations of a cloud deck at this level (Tyler et al. 1986, 1989).

Oxygen in the form of CO has been detected on both Uranus and Neptune. Millimeter-wave spectroscopy of Neptune yields about 1 ppm of CO in both the troposphere and stratosphere of Neptune (Rosenqvist et al. 1992; Marten et al. 1993). Encrenaz et al. (2004) found a CO mixing ratio of 3×10^{-8} in the lower stratosphere of Uranus from CO fluorescence in the 4.6-5.0 μm interval, along with a CO tropospheric upper limit of 2×10^{-8}. This measurement is consistent with previous millimeter-wave stratospheric CO upper limits of 3×10^{-8} (Rosenqvist et al. 1992, Marten et al. 1993). Modeling of CO diffusion from the deep interiors of these planets by Lodders and Fegley (1994) assumed tropospheric CO mixing ratios of $< 10^{-8}$ on Uranus and about 1 ppm on Neptune (Rosenqvist et al. 1992, Marten et al. 1993), resulting in supersolar O/H enrichment factors for Uranus and Neptune, respectively, of < 226 and 382 (Anders and Grevesse 1989), or < 331 and 560 (Grevesse et al. 2005). Although these values are strongly dependent on the model assumptions made for mixing rates, reaction rates, and reaction pathways, they are broadly consistent with the low gas complements based on gravity data for Uranus and Neptune. However, the vertical distribution of CO in Uranus inferred by Encrenaz et al. (2004) is more consistent with an external origin of CO—possibly contributed by meteorites or icy satellites—in which case CO is not diagnostic of the bulk oxygen enrichment of the planet. For Neptune, the extreme oxygen enrichments suggested by Lodders and Fegley (1994) are challenged by the D/H ratio measured in atmospheric methane, assuming equilibration of deuterium between HDO and CH_3D (Owen and Encrenaz 2006). A lower oxygen enrichment, comparable to that of methane, would satisfy the deuterium constraint.

OXYGEN IN OUTER PLANET SATELLITES

To assess the effects of O and C abundances on the material that condensed in the outer Solar System, the expected condensate density as a function of carbon partitioning for both the historical and newly proposed solar abundances is calculated on a uniform basis. For these calculations, the four components are: anhydrous rock (3360 kg m^{-3}); metallic sulfide/oxide phase (4800 kg m^{-3}); refractory organics (1700 kg m^{-3}); and water ice (940 kg m^{-3}). The results are plotted in Figures 4 and 5. In both figures, the vertical axis gives the material density of condensed protosolar material, including contributions from all four components mentioned above. Figure 4 shows that the condensate density increases with the fraction of carbon in the form of CO, because CO sequesters O in the gas phase and reduces the amount of water ice in the protosolar condensate. This effect is reduced if solid organics are plentiful

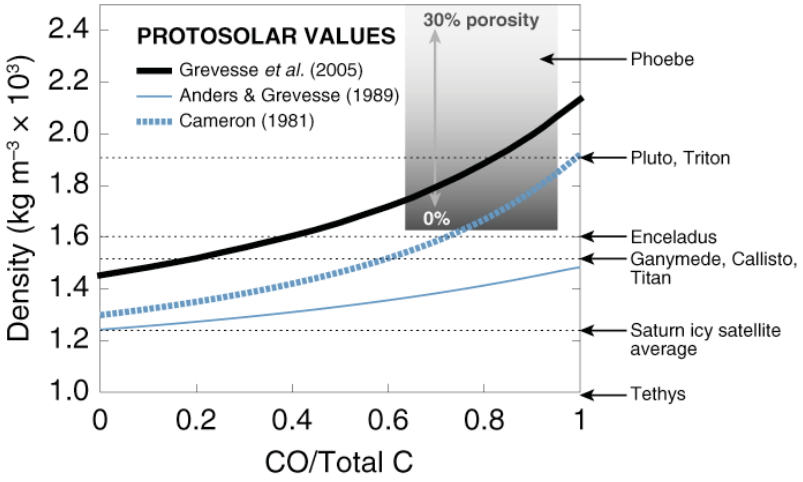

Figure 4. Model uncompressed densities of condensates in the protoplanetary disk as a function of carbon partitioning in the gas phase between CO and CH_4. Models for historical values of solar photospheric oxygen and carbon abundances are shown along with the adopted protosolar values from Grevesse et al. (2005), based on recent spectral analysis and models for photospheric compositional evolution and gravitational settling. Determinations of uncompressed density for the major icy satellites of Jupiter and Saturn (Ganymede, Callisto, and Titan) are shown as well as the outer Solar System objects Pluto and Triton. The wide and puzzling range of densities for the smaller objects in the Saturn system is illustrated by values from 1000 kg m^{-3} (Tethys) to 1600 kg m^{-3} (Enceladus) with a mass averaged value of a little over 1200 kg m^{-3}. Phoebe (probably a captured outer Solar System object) may have a density of 1600 (0% porosity) to over 2400 kg m^{-3} (~ 30% porosity) depending on its bulk porosity.

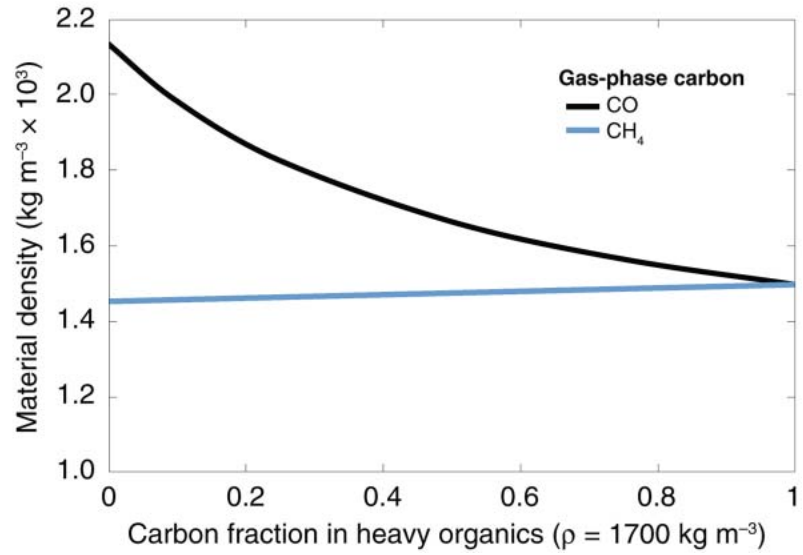

Figure 5. Protosolar condensate density versus fraction of carbon in the form of refractory organics. The refractory organics are assumed to have a mean density of 1700 kg m^{-3}, equivalent to amorphous carbon. The black line illustrates the case in which the rest of the carbon is in the form of carbon monoxide, while the shaded line illustrates the case in which it is in the form of methane. For a heavy organics fraction in excess of 0.5, the difference in density between the two cases is less than 10%. Material density is equivalent to the object density for a non-porous body small enough that compression can be neglected.

(black line in Fig. 5). But if all gas-phase carbon is in the form of CH_4 (shaded line in Fig. 5), the organic fraction has a small effect on the total condensate density, because the amount of ice in the protosolar condensate is not affected.

Jupiter's satellites

Jupiter's large Galilean satellites exhibit a strong density gradient from the innermost, Io, which is rocky and volcanic, to the outermost, Callisto. This radial density gradient is generally believed to result from the temperature gradient in the circum-Jupiter disk in which the Galilean satellites formed. Callisto's uncompressed density of 1420 kg m^{-3} (based on a modestly differentiated internal structure) belies an icier composition than its next inner neighbor, Ganymede, whose density is 1570 kg m^{-3} (McKinnon 1997; Schubert et al. 2004). Callisto's relatively undifferentiated interior also indicates a more gentle accretion history compared to Ganymede, so Callisto may be a better measure of the oxygen content of solid planetesimals in the circum-Jupiter disk. Callisto's density, which lies somewhat lower than the Ganymede-Callisto-Titan average shown in Figure 4, is consistent with solar-composition material formed in a CO-rich environment under the older solar composition tabulations (shaded curves in Fig. 4). Using the Grevesse et al. (2005) solar abundances, Callisto's density now matches that of solar composition material condensed in very CO-poor conditions, implying efficient conversion of CO to CH_4 in the circumplanetary disk.

Inward from the Galilean satellites lies the much smaller Amalthea, with a remarkably lower density of 857 ± 99 kg m^{-3}. It has been suggested that Amalthea, with its small size and low gravity, may have a large bulk porosity, similar to that attributed to several small asteroids. For a body of Amalthea's size, porosities of less than 0.4 might be reasonable and stable against compaction (Belton et al. 1995), resulting in material densities of 860 to 1400 kg m^{-3}. For material densities within this range, the moon could plausibly be constituted from material with the same uncompressed density as the outer icy satellites, requiring that Amalthea formed in a colder environment than the inner Galilean satellites, either at a different original position or at a later time when the "gas-starved" inner circumplanetary disk had cooled enough to allow ice to exist near Amalthea's current position (Anderson et al. 2005; McKinnon 2006). No evidence of water ice is seen in Amalthea's near infrared reflectance spectrum (Takato et al. 2004; Wong et al. 2006b), but this does not rule out an icy interior composition, because only the surface layer is spectroscopically sampled.

The Trojan asteroids, like Jupiter's satellites, may also share a dichotomy of origins. Densities are known for two Trojans, based on binary orbit determinations. At 2200 kg m^{-3}, the density of 624 Hektor is consistent with bulk chondritic composition, suggesting formation at its current heliocentric location (Marchis et al. 2006b). However, 617 Patroclus has a much lower bulk density, 800 kg m^{-3} (Marchis et al. 2006a). Interestingly, the few known trans-Neptunian and Kuiper belt object densities also seem to demonstrate both low- and high-density populations (see below). The densities of Hektor and Patroclus therefore may support the idea that Trojans originated in the Kuiper belt, were gravitationally scattered during the passage of Jupiter and Saturn through their 1:2 mean-motion resonance, and finally became captured in Jupiter's Lagrange points (Morbidelli et al. 2005; Tsiganis et al. 2005).

Saturn's satellites

Saturn's satellite system consists of one planet-sized moon, Titan, a collection of small and medium-sized objects usually referred to as the icy satellites, and a retinue of distant, irregular, presumably captured objects, of which Phoebe is the largest. The range in density among these objects suggests origins in regions of differing carbon chemistry and/or significant fractionation of ice and rock from solar equilibrium values. Titan has a density that is virtually identical to that of Ganymede and Callisto, and thus is consistent with an equilibrium condensate from a reducing circumplanetary disk.

However, the rest of what are usually referred to as Saturn's "icy satellites" present even more serious problems for simple equilibrium condensation models than does Amalthea in the Jupiter system. The masses and sizes of the medium to small icy satellites are now well enough known from combined spacecraft and astrometric data to confirm the large variations in their densities hinted at by early Voyager measurements and the lack of a simple radial variation in density such as is seen in the Jupiter system. Enceladus and Dione have densities similar to the uncompressed Titan value, but Iapetus, Rhea, and Tethys have significantly lower values. Estimates of the densities for the small co-orbital and ring-related satellites are even lower, below that of Amalthea. The mass-weighted average density of the icy satellites (excluding Titan) is a little over 1200 kg m^{-3} (Jacobson 2004). It is interesting to note that the original density of Enceladus decreases from Titan-like to icy satellite-like, if its current H_2O loss rate of 150 ± 30 kg s^{-1} (Tian et al. 2007) is assumed to have remained constant over the age of the Solar System. Although this assumption is highly questionable, it is clear that changes in satellites after their formation may complicate our attempts to use them to define conditions in the early Solar System.

Given the historical solar abundance values, material with the icy satellite average density could, in principle, be consistent with a CH_4-rich equilibrium chemistry, but would require fractionation or redistribution of the rock and ice to form the high- and low-density members of the group. For most of these satellites, the current abundance values are inconsistent with formation from a solar-composition source without later alteration.

Saturn's local environment was possibly enriched in water compared with the protoplanetary disk at the time that icy satellites formed, with Titan's formation in a different environment. It is possible that the formation of Saturn somehow led to a more oxygen-rich or water-rich circum-Saturnian disk relative to the protoplanetary disk (Mosqueira and Estrada 2003). Some mechanism for redistribution of the rock-rich and ice/carbon-rich fractions is again required to produce the range of observed densities. In addition, there is no direct evidence for such large amounts of solid carbon in the satellites, whose surfaces are all extremely ice-rich.

Finally, there is the possibility that Saturn's icy satellites represent the debris from past collisions, in which the components of the impactors were distributed unevenly among the resulting fragments. Canup and Ward (2006) raised the possibility that other large satellites were present early in Saturn's history and migrated inward as a result of interactions with gas in the circum-Saturnian disk. Such a situation would ensure collisional interactions, but collisions could also take place after dissipation of the circumplanetary disk if the resulting satellite system was not sufficiently stable (Chambers et al. 1996). Thus, Saturn's icy satellites may have been chipped off of Titan or another differentiated satellite that was subsequently lost to collision with Saturn.

Outer Solar System satellites and Kuiper Belt Objects

Data for other objects in the outer Solar System suggest a complex mixture of condensation and modification by planetary formation processes. The larger of Uranus' satellites have densities suggesting an average composition similar to Ganymede, Callisto and Titan, consistent with equilibrium condensation in a CH_4-dominated circumplanetary disk. As with the Saturn and Jupiter systems, however, there is at least one anomalously low-density moon, in this case Miranda, suggesting a more complex history. Neptune's large moon, Triton, is believed to be a captured object, formed in the outer parts of the protoplanetary disk. Its uncompressed density is ~1900 kg m^{-3}, making it considerably rock-rich compared with even the large satellites of Jupiter and Saturn. This is consistent with an equilibrium condensate in a CO-rich disk given the new solar C and O values (Fig. 4). A caveat is that the processes involved in Triton's supposed capture by Neptune may have altered its original volatile composition (McKinnon et al. 1995).

The uncompressed density of Pluto is also ~1900 kg m^{-3} (Stern et al. 1997), again consistent with equilibrium condensation from a CO-rich disk for the new C/H and O/H ratios. A significant enrichment of rock would be required, however, to explain this density in terms of the earlier Anders and Grevesse (1989) abundances. Eris (2003 EL61), possibly the most massive KBO known, has a density of 2200 ± 300 kg m^{-3} (Brown 2006). This density means that Eris, like Pluto, could have formed from solar-composition material in a CO-rich environment. The high densities of these objects argue against a large fraction of carbon occurring in the form of solid organics (Fig. 5).

The irregular orbit of Saturn's moon Phoebe is consistent with its origin as a captured object, so we discuss its composition here rather than in the Saturn section above. The Cassini flyby of Phoebe in June of 2003 yielded a mean density determination of 1630 ± 33 kg m^{-3} (Jacobson et al. 2004; Porco et al. 2005). This mean density would correspond to Phoebe's material density only if the satellite had zero porosity; the shaded region in Figure 4 demonstrates that higher porosities would correspond to higher material densities. For moderate porosities, Phoebe's material density overlaps with uncompressed densities of other objects formed in the outer parts of the protoplanetary disk, i.e. Pluto and Triton. These densities are consistent with disk chemistry from moderately reducing (CO ~ 0.25) to very CO rich values, with about 30% or less carbon in the form of organic solids (Fig. 5).

As more Kuiper Belt Objects are discovered, many with satellites, more data on densities are accumulating. Preliminary indications are that there may be both high-density and low-density objects represented, although some of the very low densities are for bodies so small that porosity makes an accurate estimate of the actual sample density difficult. Some of the small low-density objects may be fragments of a differentiated parent body, as suggested by work demonstrating that Eris may be a member of a collisional family of small objects with strong spectroscopic water features (Brown et al. 2007).

FORMATION OF THE OUTER PLANETS

Although there is considerable debate concerning many details of the formation of the outer planets, it is generally accepted that the three-phase core instability model of Pollack et al. (1996) is a good description of the formation mechanism of the giant planets. In the very rapid first phase, planetary embryos grow by solid accretion, until they have depleted the solids within their feeding zones. The planets then accrete solid and gaseous material at a slower and relatively constant rate, for periods lasting up to several million years. Finally, in the third stage, the planets reach a critical mass at which disk gas hydrodynamically collapses onto the core. The much lower gas fractions of Uranus and Neptune, compared with Jupiter and Saturn, are explained by their failure to reach the critical mass for runaway gas accretion before the dissipation of the protoplanetary disk.

Thus, the study of oxygen in the giant planets is primarily the study of the solid planetesimals accreted by these planets in the first two phases of their formation. But none of the bulk water abundances of the giant planets are known. Knowledge of the enrichments of the other volatile gases is an important avenue for investigating the O/H ratios of the giant planets, since the enriched abundances of these gases suggest that they were brought to the giant planets by solid planetesimals. The difficulty with this line of inquiry lies in finding a robust and plausible mechanism for trapping the volatiles in solids while providing an equally compelling explanation of the varying degrees of volatile enrichment in the giant planets. Although the precise mechanism of volatile enrichment has not been isolated, arguments have been made in favor of accretion of planetesimals composed chiefly of amorphous or crystalline ice, or even carbonaceous material. Another possibility is that the atmospheric volatile enrichments resulted from the accretion of enriched, processed gas in an evolved protoplanetary disk.

Volatile enrichment by icy planetesimals

The commonly accepted hypothesis that Jupiter accreted planetesimals composed mainly of ice seeks to explain the abundances of other volatiles through their trapping in either amorphous ice (Atreya et al. 1999; Owen et al. 1999) or crystalline ice clathrates (Gautier et al. 2001; Hersant et al. 2004). For a given heliocentric distance in the protoplanetary disk, Gautier et al. and Hersant et al. calculated the evolutionary temperature-pressure track as a function of time. As conditions changed, they described a progressive clathration of each volatile gas remaining in the disk, based on the thermodynamic review of clathration given in Lunine and Stevenson (1985). For Jupiter's case, they postulated that the disk cooled to about 35 K after 5.6 million years, sufficient to form clathrates of argon, before Jupiter reached critical mass for runaway gas accretion. Details of their disk evolution and clathration model could only match Jupiter's sulfur abundance if H_2S gas in the protoplanetary disk were reduced to 0.57 × solar (using Anders and Grevesse 1989 definitions). Hersant et al. (2004) attempt to justify the H_2S depletion by invoking inner disk processing to remove some of the gaseous H_2S, but Lodders (2004) pointed out that this mechanism would result in virtually all of the H_2S being lost to FeS, so the required factor of 0.57 selected by Hersant et al. (2004) to match Jupiter's sulfur abundance is questionable. Additionally, S/O in Comet Halley was about 0.035 in gas and dust (Mumma et al. 1993), S/O in multiple comets comes out to be about 0.028 (Irvine et al. 2000), and solar S/O is 0.03 (Grevesse et al. 2005), so evidence is lacking for subsolar sulfur in icy planetesimals. The depletion of H_2S gas prior to clathrate formation was imposed for all the giant planets studied by Hersant et al. (2004). Because each clathrate guest atom/molecule is enclosed by 5.66 or 5.75 water molecules (depending on the crystalline structure of the ice), enrichment of volatiles in Jupiter by clathrate ice accretion would imply an O/H enrichment 10.5 × solar (Anders and Grevesse 1989) or 15 × solar (Grevesse et al. 2005), at the absolute minimum. The implied O/H would be even higher if clathration were less than 100% efficient.

Amorphous ice is also capable of trapping volatiles. It is more likely that the planetesimals which formed the outer planets were themselves formed of amorphous ice grains, since this is the form taken by ice condensed from vapor at temperatures less than 130 K (Petrenko and Whitworth 1999). Wang et al. (2005) also note that the inelasticity of amorphous ice provides the "stickiness" necessary to facilitate the growth of planetesimals from grains. Amorphous ice formed at temperatures less than 35 K traps Ar, CO, CH_4, and N_2 with equal efficiency (Bar-Nun et al. 1988), while at higher temperatures the gases are less easily trapped, with different trapping efficiencies. Roughly equivalent Jovian enrichments of Ar, N, and C thus imply very low ice formation temperatures, if trapping in amorphous ice took place (Owen et al. 1999; Atreya et al. 1999; Owen and Encrenaz 2003, 2006). A low temperature of formation was also required by the scenario of Hersant et al. (2004), but the two proposed forms of ice imply differing values of the bulk water abundance in Jupiter, based on the observed volatile enrichments. Since low-temperature amorphous ice traps gas extremely efficiently, the minimum Jovian water abundance is a factor of three less than the minimum Jovian water abundance required by the clathrate mechanism.

Owen and Encrenaz (2003, 2006) took a step back from the discussion of the mechanics of volatile trapping in icy planetesimals, and simply started with the assumption that these planetesimals included everything (except hydrogen, helium, and neon) in protosolar proportions. They found that the degree of volatile enrichment in the atmospheres of all of the outer planets could be explained by the accretion of approximately 10 earth masses of these solar composition icy planetesimals (SCIPs) by each planet. This mass of solar composition condensate in each giant planet would explain observed values of D/H on Uranus and Neptune, Jupiter's heavy element enrichments, and the enrichments of carbon in all the giant planets. Some fraction of this icy mass could have built the cores of these planets—prior to directly capturing gas from the disk (e.g., Mizuno 1980, Pollack et al. 1996)—but some fraction could have been

accreted later into the gaseous envelopes (Pollack et al. 1996). If the SCIPs contributed mainly to the giant planet cores rather than to the envelopes, then this scenario requires the further assumption that volatile species are not retained in the cores, but are mixed into the gaseous envelope—an assumption that is well-justified by the similar levels of enrichment among the noble gases and the volatiles (Fig. 3). The Owen and Encrenaz (2003, 2006) scenario was not compatible with the low methane abundance for Saturn found by Kerola et al. (1997). Instead, Owen and Encrenaz (2003) predicted a higher methane abundance that was later validated by Cassini CIRS methane retrievals (Orton et al. 2005, Flasar et al. 2005). Enrichment of heavy elements via SCIPs calls for the same enrichment for oxygen (and all other heavy elements) on Saturn as is observed for carbon. Owen and Encrenaz (2003, 2006) propose that Kuiper Belt Objects may be representative of SCIPs accreted by the giant planets, provided they have remained at temperatures below 25K since the Solar System formed.

Volatile enrichment by carbonaceous planetesimals

The tarry planetesimal idea (Lodders 2004) hinges on the hypothesis that the deep water mixing ratio sampled by the GPMS was indeed characteristic of Jupiter's well-mixed water abundance. Although the considerations presented in the previous sections argue strongly against this possibility, the Lodders (2004) model at least shows that a wide diversity of conclusions can be drawn from the relatively few outer planet compositional data available. Lodders (2004) claims that during Jupiter's formation, temperatures in the local protoplanetary disk were too high for water condensation. The rapid accretion of Jupiter's core was instead driven by the accumulation of carbonaceous (or tarry) planetesimals. Because she determined that sulfur would have been accreted by Jupiter entirely in the solid phase, but has been completely converted to H_2S gas in Jupiter's troposphere, Lodders (2004) normalized abundance ratios of volatile elements in Jupiter to sulfur. This normalization yields abundances of H, He, Ne, and O that are subsolar with respect to S, while Ar, Kr, Xe, and P are solar, and C and N are supersolar.[2] Subsolar H, He, and Ne (with respect to S) are conveniently explained by sequestering them into Jupiter's metallic hydrogen region, where Lodders (2004) posits other elements are not soluble. Although the lack of a good experimental or theoretical description of the molecular to metallic hydrogen transition makes the insolubility argument difficult to resolve, one weakness of the argument is the principle that heavier things sink, so any of these heavier elements should have rained onto Jupiter's core instead of defying gravity by bubbling up into the observable atmosphere. The solar (with respect to S) abundances of the other noble gases are used as evidence that they were directly captured as gas. Supersolar C/S is the basis for the tarry planetesimal hypothesis, but supersolar N is dismissed because the N/S ratio found for Jupiter is marginally consistent, within uncertainty, with solar N/S[3]. One major problem with a subsolar O/S ratio is not addressed in this scenario, however. If oxygen was not brought to Jupiter in the form of ice (due to higher than previously suggested disk temperatures), then it should have been present, and therefore accreted, as gas. If the noble gases were accreted directly as gas while maintaining solar ratios (with respect to sulfur), then oxygen should have followed the same pattern. The tarry planetesimal idea of Lodders (2004) thus appears to be an insoluble paradox: it is based on the unsubstantiated premise that Jupiter's O/S ratio is subsolar, yet a rigorous analysis of the mechanics of the hypothesis

[2] Note that Lodders (2004) used a unique set of protosolar abundances (Lodders 2003), which featured C, N, O, Kr, and Xe protosolar abundances very similar to those in Grevesse et al. (2005), and S and Ar protosolar abundances slightly lower than the solar abundances of Anders and Grevesse (1989). However, the set of protosolar abundances chosen does not alter the major conclusion of her work.

[3] Jupiter's N/S = 7.5 ± 3.4 using GPMS mixing ratios from Wong et al. (2004), or 9.1 ± 2.1 substituting the ammonia mole fraction derived from probe radio signal attenuation by Folkner et al. (1998). Solar N/S = 4.4 using either Lodders (2003) or Grevesse et al. (2005) tabulations, which is marginally consistent with GPMS-derived N/S but not consistent with the ammonia abundance of Folkner et al. (1998).

demand that Jupiter end up with a solar O/S and supersolar O/H ratios, although the minimum consistent O/H ratio would be slightly reduced by condensation of deep silicate clouds, as in Fegley and Lodders (1994). The O/H paradox, combined with the problems discussed above concerning buoyancy of insoluble elements in metallic hydrogen and the supersolar N/S ratio, renders the tarry planetesimal hypothesis untenable, although there is no reason to rule out a carbonaceous component within the icy planetesimals favored by most other researchers.

Volatile enrichment by disk evolution

Evolutionary processes in the protoplanetary disk—including radial motion of solids, turbulent diffusion, and evaporation of the disk atmosphere—may have had strong effects on the giant planet volatile inventories. The "snow line" near 5 AU is a key landmark in this discussion. In a turbulent protoplanetary disk, diffusion of water vapor outside of the snow line would result in increased condensation near Jupiter's orbit, enhancing the concentration of ice there (Morfill and Völk 1984; Stevenson and Lunine 1988). Cuzzi and Zahnle (2004) modeled a turbulent protoplanetary disk, considering the effect of an inward flux of solid material due to gas drag on meter-sized particles (Weidenschilling 1977). For water, they concluded that the inward flux of meter-sized particles was much greater than the outward diffusive vapor flux, resulting in a snow line that behaved more like an evaporation front than the condensation front examined by Morfill and Völk (1984) and Stevenson and Lunine (1988). Large enrichments of water vapor are produced inside the snow line. With the addition of a planetesimal sink (such as Jupiter) to stop the influx of solids near the snow line, water instead becomes depleted in the inner Solar System due to outward diffusion. Although enhancements of ice abundance near the snow line help satisfy the constraint that Jupiter formed rapidly enough to capture its gas before dissipation of the protosolar disk, these scenarios do little to accelerate the formation of the other outer planets. Other volatile species would be very poorly trapped in ice formed at 5 AU by outward diffusion, so abundances of nitrogen and the noble gases would be nearly solar, at odds with Jupiter's composition. Cuzzi and Zahnle (2004) suggest that the meter-sized particles drifting inward would release other volatiles at their respective evaporation fronts, perhaps explaining Jupiter's volatile enrichments. The variation in evaporation temperatures of the noble gases, however, would result in very different enrichment factors for each gas at Jupiter, rather than the relatively constant enrichment factor observed for the noble gases (Guillot and Hueso 2006).

Instead, Guillot and Hueso (2006) proposed that photoevaporation of the protoplanetary disk would result in enriched midplane gas, which was then captured directly by the giant planets. This model is based on the protoplanetary disk evolution model of Hueso and Guillot (2005), but it includes photoevaporation driven both by extreme ultraviolet radiation from the central star in the inner (< 10 AU) disk region as well as by far ultraviolet radiation from stellar neighbors in the star-formation region. Noble gases condense on grains in the cold outer disk. Although N_2 is not discussed by Guillot and Hueso (2006), due to its low condensation temperature it would behave exactly as a noble gas in their scenario. The grains settle to the midplane and drift inward due to gas drag, releasing noble gases as they move to warmer regions of the disk. Guillot and Hueso (2006) claim that the noble gases will remain at the midplane of the disk, due to the negative vertical temperature gradient, and photoevaporation will preferentially remove H, He, and Ne, species that are gaseous at all temperatures, only from the disk atmosphere furthest from the midplane. This method enriches the midplane in noble gases, which are then directly accreted by the giant planets, and makes the potentially testable prediction that the noble gas mixing ratios should be the same on both Jupiter and Saturn. Because the accretion of enriched gas implies that the giant planets formed relatively late, this evaporation scenario also nicely limits the amount of inward migration experienced by the giant planets.

CONCLUSIONS

Oxygen, primarily in the form of water ice, is widely regarded as the milk that fed the young outer planets until they grew big enough to directly accrete disk gas. We have not yet determined the bulk oxygen abundance in any giant planet atmosphere, leaving giant planet formation models somewhat unconstrained, but future measurements may allow distinction between alternative formation scenarios.

Numerous attempts to measure Jupiter's bulk water abundance are summarized in Table 1. The GPMS measurement established that it is at least 50% of the solar value, in a region of atypical meteorology, with volatile depletions to great depths. Taking into account the meteorological and model limitations of the investigations summarized in Table 1, there is broad consistency with a solar or greater water abundance. Although the lightning depth analyses are very model-dependent, multiple investigations by separate teams all suggest supersolar water abundances. Confidence in this result is bolstered by the fact that supersolar water would ensure both liquid and solid cloud particles, greatly facilitating lightning generation.

Other volatile gases besides water have been successfully measured in Jupiter, and the methane mixing ratios are known to increase with distance from the Sun in all four outer planet atmospheres. These measurements have stimulated discussions of the details of outer planet formation. The observed methane abundances are consistent with the ideas of Owen and Encrenaz (2003, 2006), in which about ten earth masses of solar composition icy planetesimals were accreted by all the giant planets, leading to the prediction that, in each planet, the enrichments with respect to hydrogen of all the volatiles (nitrogen, oxygen, sulfur, noble gases other than neon) should be equal to the carbon enrichments. Alternately, if water enrichments are found to be at least three times greater than the enrichments of other volatiles, then accretion of volatiles trapped in water ice clathrates would be a reasonable explanation (Gautier et al. 2001, Hersant et al. 2004). If we someday find noble gas mixing ratios to be identical on all the giant planets, than accretion of volatiles in the gas phase from a chemically evolved disk would be the obvious mechanism (Guillot and Hueso 2006).

The recently updated protosolar abundance tabulations of Grevesse et al. (2005) make interpretation of Jupiter's volatile inventory (Fig. 3) more difficult than with the older Anders and Grevesse (1989) values. The exceptionally high argon enrichment is particularly challenging to account for. As the most volatile species in Figure 3, argon's larger enrichment compared to the other gases defies any enrichment process discussed in this chapter. One possible interpretation would be to consider the factor of two revision in protosolar argon to be indicative of a factor of two uncertainty in all the protosolar volatile abundances, leading to the conclusion that the GPMS measurements yield an enrichment of $4 \pm 2 \times$ solar for all the volatiles (except water). This conclusion should hopefully be robust against future improvements to the protosolar abundances.

The newly proposed values for the solar abundances of carbon and oxygen also result in a significant increase in the expected density of condensates from a solar composition disk, regardless of the state of carbon in the system. The densities of objects formed in the outer Solar System, either in the protoplanetary disk or in circumplanetary disks, are generally consistent with the density of equilibrium condensates expected for a range of carbon chemistry in these environments. A notable exception is the Saturn system, where the presence of very low-density satellites is inconsistent with equilibrium expectations and seems to require a more complex scenario with processes resulting in depletion of silicate materials, collisional disruption of differentiated satellites, or enrichment of water ice.

ACKNOWLEDGMENTS

Portions of this work were done at the University of California with support from NASA grants NAG 5-12062 and NNG 05GF09G, and at the Jet Propulsion Laboratory, Caltech, under a contract from NASA. We thank Matthew Browning for helpful discussions, and Glenn MacPherson for organizing the fascinating and interdisciplinary "Workshop on Oxygen in Earliest Solar System Materials and Processes" just outside of the Great Smoky Mountains National Park. W.B. McKinnon provided a helpful and professional review.

REFERENCES

Allende Prieto C, Lambert DL, Asplund M (2002) A reappraisal of the solar photospheric C/O ratio. Astrophys J573:L137-L140

Anders E, Grevesse N (1989) Abundances of the elements—meteoritic and solar. Geochim Cosmochim Acta 53:197-214

Anderson JD, Johnson TV, Schubert G, Asmar S, Jacobson RA, Johnston D, Lau EL, Lewis G, Moore WB, Taylor A, Thomas PC, Weinwurm G (2005) Amalthea's density is less than that of water. Science 308:1291-1293

Armstrong KR, Minton RB, Rieke GH, Low FJ (1976) Jupiter at five microns. Icarus 29:287-298

Asplund M, Grevesse N, Sauval AJ, Allende Prieto C, Kiselman D (2004) Line formation in solar granulation. IV. [O I], O I and OH lines and the photospheric O abundance. Astron Astrophys 417:751-768

Atreya SK (1986) Atmospheres and Ionospheres of the Outer Planets and their Satellites. Springer-Verlag, New York

Atreya SK, Mahaffy PR, Niemann HB, Wong MH, Owen TC (2003) Composition and origin of the atmosphere of Jupiter-an update, and implications for the extrasolar giant planets. Planet Space Sci 51:105-112

Atreya SK, Romani PN (1985) Photochemistry and clouds of Jupiter, Saturn and Uranus. *In:* Planetary Meteorology. Hunt GE (ed) Cambridge University Press, Cambridge, p 17-68

Atreya SK, Wong A-S (2005) Coupled clouds and chemistry of the giant planets—A case for multiprobes. Space Sci Rev 116:121-136

Atreya SK, Wong MH, Owen TC, Mahaffy PR, Niemann HB, de Pater I, Drossart P, Encrenaz T (1999) A comparison of the atmospheres of Jupiter and Saturn: Deep atmospheric composition, cloud structure, vertical mixing, and origin. Planet Space Sci 47:1243-1262

Baines KH, Carlson RW, Kamp LW (2002) Fresh ammonia ice clouds in Jupiter. I. Spectroscopic identification, spatial distribution, and dynamical implications. Icarus 159:74-94

Baines KH, Mickelson ME, Larson LE, Ferguson DW (1995) The abundances of methane and ortho/para hydrogen on Uranus and Neptune: Implications of new laboratory 4-0 H2 quadrupole line parameters. Icarus 114:328-340

Banfield D, Gierasch PJ, Bell M, Ustinov E, Ingersoll AP, Vasavada AR, West RA, Belton MJS (1998) Jupiter's cloud structure from Galileo imaging data. Icarus 135:230-250

Bar-Nun A, Kleinfeld I, Kochavi E (1988) Trapping of gas mixtures by amorphous water ice. Phys Rev B 38:7749-7754

Belton M, Chapman C, Thomas P, Davies M, Greenberg R, Klaasen K, Byrnes D, D'Amario L, Synnott S, Merline W, Petit J.-M, Storrs A, Zellner B (1995) The bulk density of asteroid 243 Ida from Dactyl's orbit. Nature 374:785-788

Bézard B, Lellouch E, Strobel D, Maillard J-P, Drossart P (2002) Carbon monoxide on Jupiter: Evidence for both internal and external sources. Icarus 159:95-111

Bjoraker GL, Larson HP, Kunde VG (1986a) The abundance and distribution of water vapor in Jupiter's atmosphere. Astrophys J 311:1058-1072

Bjoraker GL, Larson HP, Kunde VG (1986b) The gas composition of Jupiter derived from 5 micron airborne spectroscopic observations. Icarus 66:579-609

Borucki WJ, Bar-Nun A, Scarf FL, Look AF, Hunt GE (1982) Lightning activity on Jupiter. Icarus 52:492-502

Borucki WJ, McKay CP, Jebens D, Lakkaraju HS, Vanajakshi CT (1996) Spectral irradiance measurements of simulated lightning in planetary atmospheres. Icarus 123:336-344

Borucki WJ, Williams MA (1986) Lightning in the Jovian water cloud. J Geophys Res 91:9893-9903

Brown ME (2006) The largest Kuiper Belt objects. Bull Am Astron Soc 38:550

Brown ME, Barkume KM, Ragozzine D, Schaller EL (2007) A collisional family of icy objects in the Kuiper belt. Nature 446:294-296

Buriez JC, de Bergh C (1981) A study of the atmosphere of Saturn based on methane line profiles near 1.1 microns. Astron Astrophys 94:382-390

Cameron AGW (1981) Elementary and nuclidic abundances in the solar system. *In:* Essays in Nuclear Astrophysics. Barns CA, Clayton DD, Schramm DN (eds) Cambridge University Press, New York, p 23-43

Canup RM, Ward WR (2006) A common mass scaling for satellite systems of gaseous planets. Nature 441:834-839

Carlson BE, Lacis AA, Rossow WB (1993) Tropospheric gas composition and cloud structure of the Jovian North Equatorial Belt. J Geophys Res 98:5251-5290

Chambers JE, Wetherill GW, Boss AP (1996) The stability of multi-planet systems. Icarus 119:261-268

Christensen-Dalsgaard J (2006) Prospects for helio- and asteroseismology. *In:* Proc. SOHO 18 / GONG 2006 / HELAS I Conference: Beyond the spherical Sun. Fletcher K (ed), ESA SP-624, CD-ROM, p 41.1

Cook AF, II Duxbury TC, Hunt GE (1979) First results on Jovian lightning. Nature 280:794

Courtin R, Gautier D, Marten A, Bezard B, Hanel R (1984) The composition of Saturn's atmosphere at northern temperate latitudes from Voyager IRIS spectra—NH_3, PH_3, C_2H_2, C_2H_6, CH_3D, CH_4, and the Saturnian D/H isotopic ratio. Astrophys J 287:899-916

Coustenis A, Salama A, Lellouch E, Encrenaz T, Bjoraker GL, Samuelson RE, de Graauw T, Feuchtgruber H, Kessler MF (1998) Evidence for water vapor in Titan's atmosphere from ISO/SWS data. Astron Astrophys 336:L85-L89

Cuzzi JN, Zahnle KJ (2004) Material enhancement in protoplanetary nebulae by particle drift through evaporation fronts. Astrophys J 614:490-496

De Graauw T, Feuchtgruber H, Bézard B, Drossart P, Encrenaz T, Beintema DA, Griffin M, Heras A, Kessler M, Leech K, Lellouch E, Morris P, Roelfsema PR, Roos-Serote M, Salama A, Vandenbussche B, Valentijn EA, Davis GR, Naylor DA (1997) First results of ISO-SWS observations of Saturn: detection of CO_2, CH_3C_2H, C_4H_2 and tropospheric H_2O. Astron Astrophys 321:L13-L16

de Pater I, Dickel JR (1991) Multifrequency radio observations of Saturn at ring inclination angles between 5 and 26 degrees. Icarus 94:474-492

Drake JJ, Testa P (2005) The "solar model problem" solved by the abundance of neon in nearby stars. Nature 436:525-528

Drossart P, Encrenaz T (1982) The abundance of water on Jupiter from the Voyager IRIS data at 5 microns. Icarus 52:483-491

Dyudina UA, del Genio AD, Ingersoll AP, Porco CC, West RA, Vasavada AR, Barbara JM (2004) Lightning on Jupiter observed in the H_α line by the Cassini imaging science subsystem. Icarus 172:24-36

Dyudina UA, Ingersoll AP, Vasavada AR, Ewald SP, The Galileo SSI Team (2002) Monte Carlo radiative transfer modeling of lightning observed in Galileo images of Jupiter. Icarus 160:336-349

Encrenaz T, Hardorp J, Owen T, Woodman J (1974) Observational constraints on model atmospheres for Uranus and Neptune. *In:* Proc. IAU Symposium 65, Exploration of the Planetary Systems. Woszczyk A, Iwaniszzwska C (eds) Kluwer/Springer, Dordrecht, p 487-496

Encrenaz T, Lellouch E, Drossart P, Feuchtgruber H, Orton GS, Atreya SK (2004) First detection of CO in Uranus. Astron Astrophys 413:L5-L9

Fegley BJ, Lodders K (1994) Chemical models of the deep atmospheres of Jupiter and Saturn. Icarus 110:117-154

Feuchtgruber H, Lellouch E, de Graauw T, Bézard B, Encrenaz T, Griffin M (1997) External supply of oxygen to the atmospheres of the giant planets. Nature 39:159-162

Flasar FM, Achterberg RK, Conrath BJ, Pearl JC, Bjoraker GL, Jennings DE, Romani PN, Simon-Miller AA, Kunde VG, Nixon CA, Bézard B, Orton GS, Spilker LJ, Spencer JR, Irwin PGJ, Teanby NA, Owen TC, Brasunas J, Segura ME, Carlson RC, Mamoutkine A, Gierasch PJ, Schinder PJ, Showalter MR, Ferrari C, Barucci A, Courtin R, Coustenis A, Fouchet T, Gautier D, Lellouch E, Marten A, Prangé R, Strobel DF, Calcutt SB, Read PL, Taylor FW, Bowles N, Samuelson RE, Abbas MM, Raulin F, Ade P, Edgington S, Pilorz S, Wallis B, Wishnow EH (2005) Temperatures, winds, and composition in the Saturnian System. Science 307:1247-1251

Folkner WM, Woo R, Nandi S (1998) Ammonia abundance in Jupiter's atmosphere derived from the attenuation of the Galileo probe's radio signal. J Geophys Res 103:22847-22856

Friedson AJ (2005) Water, ammonia, and H_2S mixing ratios in Jupiter's five-micron hot spots: A dynamical model. Icarus 177:1-17

Gautier D, Bezard B, Marten A, Baluteau JP, Scott N, Chedin A, Kunde V, Hanel R (1982) The C/H ratio in Jupiter from the Voyager infrared investigation. Astrophys J 257:901-912

Gautier D, Hersant F, Mousis O, Lunine JI (2001) Enrichment in volatiles in Jupiter: A new interpretation of the Galileo measurements. Astrophys J 550:L227-L230

Gierasch PJ, Ingersoll AP, Banfield D, Ewald SP, Helfenstein P, Simon-Miller A, Vasavada A, Breneman HH, Senske DA, A4 Galileo Imaging Team (2000) Observation of moist convection in Jupiter's atmosphere. Nature 403:628-630

Grevesse N, Asplund M, Sauval AJ (2005) The new solar chemical composition. *In:* Element Stratification of Stars, 40 years of Atomic Diffusion (EAS Publications Series 17). Alecian G, Richard O, Vauclair S (eds) EDP Sciences, Les Ulis France, p 21-30

Guillot T (2006) Physics of substellar objects interiors, atmospheres, evolution. *In:* Extrasolar planets, Saas-Fee Advanced Course 31. Cassen P, Guillot T, Quirrenbach A (eds) Springer, New York, p 243-368

Guillot T, Hueso R (2006) The composition of Jupiter: sign of a (relatively) late formation in a chemically evolved protosolar disc. Mon Not R Astron Soc 367:L47-L51

Hersant F, Gautier D, Lunine JI (2004) Enrichment in volatiles in the giant planets of the Solar System. Planet Space Sci 52:623-641

Hubbard WB, Podolak M, Stevenson DJ (1995) The interior of Neptune. *In:* Neptune and Triton. Cruikshank DP (ed) University of Arizona Press, Tucson, p 109-138

Hueso R, Guillot T (2005) Evolution of protoplanetary disks: constraints from DM Tauri and GM Aurigae. Astron Astrophys 442:703-725

Irvine WM, Schloerb FP, Crovisier J, Fegley B Jr, and Mumma MJ, (2000) Comets: a link between interstellar and nebular chemistry. *In:* Protostars and Planets IV. Mannings V, Boss AP, Russell SS (eds) University of Arizona Press, Tucson, p 1159-1200

Irwin PGJ, Weir AL, Smith SE, Taylor FW, Lambert AL, Calcutt SB, Cameron-Smith PJ, Carlson RW, Baines K, Orton GS, Drossart P, Encrenaz T, Roos-Serote M (1998) Cloud structure and atmospheric composition of Jupiter retrieved from Galileo near-infrared mapping spectrometer real-time spectra. J Geophys Res 103:23001-23022

Irwin PGJ, Weir AL, Taylor FW, Calcutt SB, Carlson RW (2001) The origin of belt/zone contrasts in the atmosphere of Jupiter and their correlation with 5-μm opacity. Icarus 149:397-415

Jacobson RA (2004) The orbits of the major Saturnian satellites and the gravity field of Saturn from spacecraft and Earth-based observations. Astron J 18:492-501

Jacobson RA, Antreasian PG, Bordi JJ, Criddle KE, Ionasescu R, Jones JB, Meek MC, Owen WM, Jr, Roth DC, Roundhill IM, Stauch JR, Cassini Navigation (2004) The orbits of the major Saturnian satellites and the gravity field of the Saturnian system. Bull Am Astron Soc 36:1097

Karkoschka E, Tomasko MG (1992) Saturn's upper troposphere 1986-1989. Icarus 97:161-181

Keay CSL, Low FJ, Rieke GH, Minton RB (1973) High-resolution maps of Jupiter at 5 microns. Astrophys J 183:1063-1074

Kerola DX, Larson HP, Tomasko MG (1997) Analysis of the near-IR spectrum of Saturn: A comprehensive radiative transfer model of its middle and upper troposphere. Icarus 127:190-212

Knacke RF, Kim SJ, Ridgway ST, Tokunaga AT (1982) The abundances of CH_4, CH_3D, NH_3, and PH_3 in the troposphere of Jupiter derived from high-resolution 1100-1200/cm spectra. Astrophys J 262:388-395

Kunde V, Hanel R, Maguire W, Gautier D, Baluteau JP, Marten A, Chedin A, Husson N, Scott N (1982) The tropospheric gas composition of Jupiter's north equatorial belt (NH_3, PH_3, CH_3D, GeH_4, H_2O) and the Jovian D/H isotopic ratio. Astrophys J 263:443-467

Kunde VG, Flasar FM, Jennings DE, Bézard B, Strobel DF, Conrath BJ, Nixon CA, Bjoraker GL, Romani PN, Achterberg RK, Simon-Miller AA, Irwin P, Brasunas JC, Pearl JC, Smith MD, Orton GS, Gierasch PJ, Spilker LJ, Carlson RC, Mamoutkine AA, Calcutt SB, Read PL, Taylor FW, Fouchet T, Parrish P, Barucci A, Courtin R, Coustenis A, Gautier D, Lellouch E, Marten A, Prangé R, Biraud Y, Ferrari C, Owen TC, Abbas MM, Samuelson RE, Raulin F, Ade P, Césarsky CJ, Grossman KU, Coradini A (2004) Jupiter's atmospheric composition from the Cassini thermal infrared spectroscopy experiment. Science 305:1582-1587

Lellouch E, Bézard B, Moses JI, Davis GR, Drossart P, Feuchtgruber H, Bergin EA, Moreno R, Encrenaz T (2002) The origin of water vapor and carbon dioxide in Jupiter's atmosphere. Icarus 159:112-131

Lellouch E, Drossart P, Encrenaz T (1989a) A new analysis of the Jovian 5-micron Voyager/IRIS spectra. Icarus 77:457-465

Lellouch E, Drossart P, Encrenaz T (1989b) Erratum: A new analysis of the Jovian 5-μm Voyager/IRIS Spectra. Icarus 80:224

Levin Z, Borucki WJ, Toon OB (1983) Lightning generation in planetary atmospheres. Icarus 56:80-115

Li L, Ingersoll AP, Vasavada AR, Porco CC, del Genio AD, Ewald SP (2004) Life cycles of spots on Jupiter from Cassini images. Icarus 172:9-23

Lindal GF (1992) The atmosphere of Neptune - an analysis of radio occultation data acquired with Voyager 2. Astron J 103:967-982

Lindal GF, Lyons JR, Sweetnam DN, Eshleman VR, Hinson DP (1987) The atmosphere of Uranus - Results of radio occultation measurements with Voyager 2. J Geophys Res 92:14987-15001

Linke WF (1965*)* Solubilities of Inorganic and Metalorganic Compounds. 4th edition. American Chemical Society, Washington DC

Little B, Anger CD, Ingersoll AP, Vasavada AR, Senske DA, Breneman HH, Borucki WJ, The Galileo SSI Team (1999) Galileo images of lightning on Jupiter. Icarus 142:306-323

Lodders K (2003) Solar System abundances and condensation temperatures of the elements. Astrophys J 591:1220-1247
Lodders K (2004) Jupiter formed with more tar than ice. Astrophys J 611:587-597
Lodders K, Fegley B Jr. (1994) The origin of carbon monoxide in Neptune's atmosphere. Icarus 112:368-375
Lunine JI, Hunten DM (1987) Moist convection and the abundance of water in the troposphere of Jupiter. Icarus 69:566-570
Lunine JI, Stevenson DJ (1985) Thermodynamics of clathrate hydrate at low and high pressures with application to the outer solar system. Astrophys J Suppl Ser 58:493-531
Lutz BL, Owen TC, Cess RD (1976) Laboratory band strengths of methane and their application to the atmospheres of Jupiter, Saturn, Uranus, Neptune and Titan. Astrophys J 203:541-551
Mahaffy PR, Niemann HB, Alpert, A, Atreya SK, Demick, J, Donahue TM, Harpold DN, Owen TC (2000) Noble gas abundance and isotope ratios in the atmosphere of Jupiter from the Galileo probe mass spectrometer. J Geophys Res Planets 105:15,061-15,072
Mahaffy PR, Niemann HB, Demick JE (1999) Measurement of ammonia at Jupiter with the Galileo Probe Mass Spectrometer. Bull Am Astron Soc 31:1154
Marchis F, Berthier J, Wong MH, Descamps P, Hestroffer D, Colas F, de Pater I, Vachier F (2006b) Search of binary Jupiter-Trojan asteroids with laser guide star AO systems: A moon around 624 Hektor. Bull Am Astron Soc 38:615
Marchis F, Hestroffer D, Descamps P, Berthier J, Bouchez AH, Campbell RD, Chin JCY, van Dam MA, Hartman SK, Johansson EM, Lafon RE, Le Mignant D, de Pater I, Stomski PJ, Summers DM, Vachier F, Wizinovich PL, Wong MH (2006a) A low density of 0.8 g cm^{-3} for the Trojan binary asteroid 617 Patroclus. Nature 439:565-567
Marten A, Gautier D, Owen T, Sanders DB, Matthews HE, Atreya SK, Tilanus RPJ, Deane JR (1993) First observations of CO and HCN on Neptune and Uranus at millimeter wavelengths and their implications for atmospheric chemistry. Astrophys J 406:285-297
McKinnon WB (2006) Formation and early evolution of Io. *In:* Io after Galileo. Lopes RC, Spencer JR (eds) Springer-Praxis, New York, p 61-88
McKinnon WB (1997) Mystery of Callisto: Is it undifferentiated? Icarus 130:540-543
McKinnon WB, Lunine JI, Banfield D (1995) Origin and evolution of Triton. *In:* Neptune and Triton. Cruikshank DP (ed) University of Arizona Press, Tucson, p 807-878
Mizuno H (1980) Formation of the giant planets. Prog Theor Phys 64:544-557
Morbidelli A, Levison HF, Tsiganis K, Gomes R (2005) Chaotic capture of Jupiter's Trojan asteroids in the early Solar System. Nature 435:462-465
Morfill GE, Völk HJ (1984) Transport of dust and vapor and chemical fractionation in the early protosolar cloud. Astrophys J 287:371-395
Mosqueira I, Estrada PR (2003) Formation of the regular satellites of giant planets in an extended gaseous nebula II: satellite migration and survival. Icarus 163:232-255
Mumma MJ, Weissman PR, Stern SA (1993) Comets and the origin of the solar system—Reading the Rosetta Stone. *In:* Protostars and Planets III. Levy EH, Lunine JI (eds) University of Arizona Press, Tucson, p 1177-1252
Niemann HB, Atreya SK, Carignan GR, Donahue TM, Haberman JA, Harpold DN, Hartle RE, Hunten DM, Kasprzak WT, Mahaffy PR, Owen TC, Spencer NW, Way SH (1996) The Galileo probe mass spectrometer: composition of Jupiter's atmosphere. Science 272:846-849
Niemann HB, Atreya SK, Carignan GR, Donahue TM, Haberman JA, Harpold DN, Hartle RE, Hunten DM, Kasprzak WT, Mahaffy PR, Owen TC, Way SH (1998) The composition of the Jovian atmosphere as determined by the Galileo probe mass spectrometer. J Geophys Res 103:22831-22846
Nixon CA, Irwin PGJ, Calcutt SB, Taylor FW, Carlson RW (2001) Atmospheric composition and cloud structure in Jovian 5-μm hotspots from analysis of Galileo NIMS measurements. Icarus 150:48-68
Noll KS, Gilmore D, Knacke RF, Womack M, Griffith CA, Orton G (1997) Carbon monoxide in Jupiter after Comet Shoemaker-Levy 9. Icarus 126:324-335
Noll KS, Knacke RF, Geballe TR, Tokunaga AT (1988) The origin and vertical distribution of carbon monoxide in Jupiter. Astrophys J 324:1210-1218
Orton GS, Fisher BM, Baines KH, Stewart ST, Fiedson AJ, Ortiz JL, Marinova M, Ressler M, Dayal A, Hoffman W, Hora J, Hinkley S, Krishnan V, Masanovic M, Tesic J, Tziolas A, Parija KC (1998) Characteristics of the Galileo probe entry site from Earth-based remote sensing observations. J Geophys Res 103:22791-22814
Orton G, Fletcher L, Irwin P, Bjoraker G, Flasar FM, Wishnow E (2005) The super-solar abundance of methane in Saturn from Cassini CIRS spectra. Geophys Res Abstr 7:05823
Owen T (1967) Comparisons of laboratory and planetary spectra. IV. The identification of the 7500-Å bands in the spectra of Uranus and Neptune. Icarus 6:108-113
Owen T, Encrenaz T (2003) Element abundances and isotope ratios in the giant planets and Titan. Space Sci Rev 106:121-138

Owen T, Encrenaz T (2006) Compositional constraints on giant planet formation. Planet Space Sci 54:1188-1196

Owen T, Mahaffy P, Niemann HB, Atreya S, Donahue T, Bar-Nun A, de Pater I (1999) A low-temperature origin for the planetesimals that formed Jupiter. Nature 402:269-270

Petrenko VF, Whitworth RW (1999) Physics of Ice. Oxford University Press, New York

Podolak M, Podolak JI, Marley MS (2000) Further investigations of random models of Uranus and Neptune. Planet Space Sci 48:143-151

Pollack JB, Hubickyj O, Bodenheimer P, Lissauer JJ, Podolak M, Greenzweig Y (1996) Formation of the giant planets by concurrent accretion of solids and gas. Icarus 124:62-85

Porco CC, Baker E, Barbara J, Beurle K, Brahic A, Burns JA, Charnoz S, Cooper N, Dawson DD, Del Genio AD, Denk T, Dones L, Dyudina U, Evans MW, Giese B, Grazier K, Helfenstein P, Ingersoll AP, Jacobson RA, Johnson TV, McEwen A, Murray CD, Neukum G, Owen WM, Perry J, Roatsch T, Spitale J, Squyres S, Thomas PC, Tiscareno M, Turtle E, Vasavada AR, Veverka J, Wagner R, West R (2005) Cassini imaging science: Initial results on Phoebe and Iapetus. Science 307:1237-1242

Prinn RG (1993) Chemistry and evolution of gaseous circumstellar disks. *In:* Protostars and Planets III. Levy EH, Lunine JI (eds) University of Arizona Press, Tucson, p 1005-1028

Roos-Serote M, Atreya SK, Wong MH, Drossart P (2004) On the water abundance in the atmosphere of Jupiter. Planet Space Sci 52:397-414

Roos-Serote M, Drossart P, Encrenaz T, Carlson RW, Leader F (1999) Constraints on the tropospheric cloud structure of Jupiter from Spectroscopy in the 5-μm region: A comparison between Voyager/IRIS, Galileo-NIMS, and ISO-SWS Spectra. Icarus 137:315-340

Roos-Serote M, Drossart P, Encrenaz T, Lellouch E, Carlson RW, Baines KH, Kamp L, Mehlman R, Orton GS, Calcutt S, Irwin P, Taylor F, Weir A (1998) Analysis of Jupiter North Equatorial Belt hot spots in the 4-5-μm range from Galileo/Near-Infrared Mapping Spectrometer observations: Measurements of cloud opacity, water, and ammonia. J Geophys Res 103:23023-23042

Roos-Serote M, Vasavada AR, Kamp L, Drossart P, Irwin P, Nixon C, Carlson RW (2000) Proximate humid and dry regions in Jupiter's atmosphere indicate complex local meteorology. Nature 405:158-160

Rosenqvist J, Lellouch E, Romani P, Paubert G, Encrenaz T (1992) Millimeter observations of Saturn, Uranus and Neptune: CO and HCN. Astrophys J 392:L99-L102

Sault RJ, Engel C, de Pater I (2004) Longitude-resolved imaging of Jupiter at λ=2 cm. Icarus 168:336-343

Schubert G, Anderson JD, Spohn T, McKinnon WB (2004) Interior composition, structure and dynamics of the Galilean satellites. *In*: Jupiter: The Planet, Satellites and Magnetosphere 281-306. Bagenal F, Dowling T, McKinnon WB (eds) Cambridge University Press, New York, p 281-306

Schubert G, Spohn T, Reynolds RT (1986) Thermal histories, compositions, and internal structures of the moons of the solar system. *In:* Satellites. Burns JA, Matthews MS (eds) University of Arizona Press, Tucson p 224-292

Seiff A, Kirk DB, Knight TCD, Young RE, Mihalov JD, Young LA, Milos FS, Schubert G, Blanchard RC, Atkinson D (1998) Thermal structure of Jupiter's atmosphere near the edge of a 5-μm hot spot in the north equatorial belt. J Geophys Res 103:22857-22890

Showman AP, Dowling TE (2000) Nonlinear simulations of Jupiter's 5-micron hot spots. Science 289:1737-1740

Simonelli DP, Pollack JB, McKay CP, Reynolds RT, Summers AL (1989) The carbon budget in the outer solar nebula. Icarus 82:1-35

Slipher VM (1933) Spectrographic studies of the planets (George Darwin Lecture). Mon Not R Astron Soc 93:657-668

Smith BA, Soderblom LA, Johnson TV, Ingersoll AP, Collins SA, Shoemaker EM, Hunt GE, Masursky H, Carr MH, Davies ME, Cook AF, Boyce JM, Owen T, Danielson GE, Sagan C, Beebe RF, Veverka J, McCauley JF, Strom RG, Morrison D, Briggs GA, Suomi VE (1979) The Jupiter system through the eyes of Voyager 1. Science 204:951-957

Stern SA, McKinnon WB, Lunine JI (1997) On the origin of Pluto, Charon, and the Pluto-Charon Binary. *In:* Pluto and Charon. Stern SA, Tholen DJ (eds) University of Arizona Press, Tucson AZ, p. 605-663.

Stevenson DJ, Lunine JI (1988) Rapid formation of Jupiter by diffuse redistribution of water vapor in the solar nebula. Icarus 75:146-155

Takato N, Bus SJ, Terada H, Pyo T-S, Kobayashi N (2004) Detection of a deep 3-μm absorption feature in the spectrum of Amalthea (JV). Science 306:2224-2227

Tian F, Stewart AIF, Toon OB, Larsen KW, Esposito LW (2007) Monte Carlo simulations of the water vapor plumes on Enceladus. Icarus 188:154-161

Tsiganis K, Gomes R, Morbidelli A, Levison HF (2005) Origin of the orbital architecture of the giant planets of the Solar System. Nature 435:459-461

Turcotte S, Richer J, Michaud G, Iglesias CA, Rogers FJ (1998) Consistent solar evolution model including diffusion and radiative acceleration effects. Astrophys J 504:539-558

Turcotte S, Wimmer-Schweingruber RF (2002) Possible *in situ* tests of the evolution of elemental and isotopic abundances in the solar convection zone. J Geophys Res 107:1442-1452

Tyler GL, Eshleman VR, Hinson DP, Marouf EA, Simpson RA, Sweetnam DN, Anderson JD, Campbell JK, Levy GS, Lindal GF (1986) Voyager 2 radio science observations of the Uranian system: Atmosphere, rings, and satellites. Science 233:79-84

Tyler GL, Sweetnam DN, Anderson JD, Borutzki SE, Campbell JK, Kursinski ER, Levy GS, Lindal GF, Lyons JR, Wood GE (1989) Voyager radio science observations of Neptune and Triton. Science 246:1466-1473

Wang H, Bell RC, Iedema MJ, Tsekouras AA, Cowin JP (2005) Sticky ice grains aid planet formation: Unusual properties of cryogenic water ice. Astrophys J 620:1027-1032

Weidenschilling SJ (1977) Aerodynamics of solid bodies in the solar nebula. Mon Not R Astron Soc 180:57-70

Weidenschilling SJ, Lewis JS (1973) Atmospheric and cloud structures of the Jovian planets. Icarus 20:465-476

Westphal JA (1969) Observations of localized 5-micron radiation from Jupiter. Astrophys J 157:L63-L64

Wilson JA (1925) The total and partial vapor pressures of aqueous ammonia solutions. Univ III Eng Exp Sta Bull 146

Wong MH (2001) Hydrocarbons and condensable volatiles of Jupiter's Galileo probe entry site. PhD Dissertation, University of Michigan, Ann Arbor, Michigan

Wong MH, de Pater I, Sault RJ, Lockwood S, Marchis F (2006a) Comprehensive Jupiter ammonia map. Bull Amer Astron Soc 38:#11.11

Wong MH, de Pater I, Showalter MR, Roe HG, Macintosh B, Verbanac G (2006b) Ground-based near infrared spectroscopy of Jupiter's ring and moons. Icarus 185:403-415

Wong MH, Mahaffy PR (2001) Revised deep water mixing ratio in the Galileo probe entry site from GPMS measurements. Bull Am Astron Soc 33:1043

Wong MH, Mahaffy PR, Atreya SK, Niemann HB, Owen TC (2004) Updated Galileo probe mass spectrometer measurements of carbon, oxygen, nitrogen, and sulfur on Jupiter. Icarus 171:153-170